Engineering 59 (2026) 60–81

Contents lists available at ScienceDirect

Engineering

journal homepage: www.elsevier.com/locate/eng

Research
Low Carbon Transformation for Conventional Energies—Review

Recent Research Progress in Combustion Kinetics of Biomass-Derived Oxygenated Fuels

Xiao Liu [a], Chung K. Law [a,b], Bin Yang [a,*]

[a] Center for Combustion Energy and Department of Energy and Power Engineering, Tsinghua University, Beijing 100084, China
[b] Department of Mechanical and Aerospace Engineering, Princeton University, Princeton, NJ 08544, USA

ARTICLE INFO

Article history:
Received 12 May 2025
Revised 17 September 2025
Accepted 19 October 2025
Available online 23 October 2025

Keywords:
Biofuel
Oxygenated fuels
Combustion kinetics
Gas-phase oxidation
Detailed kinetic models

ABSTRACT

Biofuels are promising alternatives to fossil fuels due to diminishing reserves and increasing environmental concerns. This review focuses on recent progress in understanding the combustion kinetics of oxygenated biofuels derived from biomass. The review begins with fundamental concepts and research methodologies in reaction kinetics, intended as a primer for engineering researchers. Subsequently, kinetic studies from the past decade on typical oxygenated biofuels are summarized, including alcohols, fatty acid methyl esters (FAMEs), ketones, ethers, and carbonates. Emphasis is placed on the influence of different oxygenated functionalities and their positions within the molecule on combustion characteristics and reaction pathways. Distinct reaction patterns for each class are highlighted. Alcohols exhibit a characteristic unimolecular dehydration reaction. FAME kinetics are similar to long-chain hydrocarbons, with unsaturation significantly impacting low-temperature oxidation. Ketone oxidation is influenced by the formation of resonance-stabilized radicals, while straight-chain ethers demonstrate a unique double negative temperature coefficient (NTC) behavior. Carbonates, relevant to lithium-ion battery safety, have gained research attention and can undergo a distinctive reaction pathway identified as CO_2 elimination reaction. To advance predictive kinetic models for biomass-derived oxygenated fuels, several targeted research directions are essential. First, there is a critical need to expand experimental datasets that capture the combustion behavior of diverse oxygenated compounds, particularly under low-temperature conditions. This must be coupled with enhanced combustion diagnostics capable of resolving key reaction intermediates characteristic of oxygenated fuel oxidation. Second, detailed quantum chemical calculations and theoretical explorations of potential energy surfaces are required to accurately determine reaction rate parameters for oxygen-involved pathways, which are often determinant in fuel decomposition and pollutant formation. Finally, progress in model predictability will depend on the adoption of advanced computational methods, including automated mechanism generation for complex oxygenated structures, systematic optimization frameworks leveraging experimental data, and the incorporation of physics-informed artificial intelligence approaches tailored to oxygenated fuel chemistries.

1. Introduction

Industrial progress has significantly enhanced production capabilities and the quality of life. Concurrently, issues pertaining to energy scarcity and climate change have progressively emerged as subjects of critical concern. The Energy Institute (EI) reports that fossil fuels, including oil, coal, and natural gas, remain the foundation of global primary energy consumption, making up 84% of the energy mix in 2023 [1]. Consequently, the world is facing an energy crisis due to the finite nature of these resources and the gradual exhaustion of energy reserves [2]. Additionally, the widespread use of fossil fuels has led to an increase in atmospheric CO_2 levels, contributing to global warming, the melting of glaciers, and rising sea levels [3]. Mitigating greenhouse gas emissions and addressing energy challenges are critical issues facing humanity.

In response to energy conservation and environmental protection, numerous nations have implemented regulations to curb fossil fuel usage and minimize pollutant emissions from vehicles

* Corresponding author.
E-mail address: byang@tsinghua.edu.cn (B. Yang).

https://doi.org/10.1016/j.eng.2025.10.012

[4–7]. In addition to improvements in car engines and exhaust after-treatment technology to reduce emissions [8,9], scientists are actively working on developing clean and renewable energy sources to decrease the reliance on fossil fuels [10]. However, these sources all face the challenges of intermittent production and geographical dependence [11], necessitating the storage of energy in secondary energy carriers through processing to meet utilization demands [12]. In recent years, considerable interest has been focused on three types of secondary energy carriers: solar fuel [13], electric fuel (e-fuel) [14], and biomass fuel (biofuel) [15]. The production of biofuels and e-fuels is derived from carbon dioxide and emits an equivalent quantity of carbon dioxide upon combustion, thereby maintaining carbon neutrality throughout their life cycle. Relative to e-fuels, biofuels can be obtained from processing various feedstocks such as plant, algae, or animal waste, and thereby have the advantages of raw materials and costs [16]. Numerous nations have enacted laws endorsing biofuels to address potential future transportation demands [17]. The International Energy Agency (IEA) anticipates that by 2025, biofuels will account for approximately 5.4% of the energy needed for road transportation [18]. Besides, from an economic and energy security perspective, the integration of biofuels will decrease a country's dependence on traditional petroleum imports from abroad and boost the domestic economy [16,19].

Biofuels have developed rapidly in the past few decades. Depending on raw materials and methodology, biofuels can be categorized into several classes designated as first, second, third, and fourth generation. The first generation of biofuels, such as biomethanol, bioethanol, and biodiesel, are produced using agricultural products. The process of fermenting crops to produce this generation has reached a considerable level of technical maturity [20]. However, it has been subject to scrutiny regarding the competition between biofuel feedstocks and foods [21–23]. Due to the limitation, research focus has been increasingly shifting towards second-generation biofuels that utilize forest, agricultural, and municipal waste as feedstocks, which are more cost-effective and readily accessible [24–26]. Regarding production methods, utilizing lignocellulose as an example, the primary approaches encompass biological and thermochemical processes [27]. The third-generation biofuels represent a fuel production technology based on algae, which are aquatic photosynthetic microorganisms that exhibit rapid growth in saline water, coastal seawater, municipal sewage, or land unsuitable for agricultural purposes and cultivation [28,29]. Biofuels produced in this way are highly carbon-neutral. According to Chisti [30], the process of cultivating 1 kg of microalgae can sequester up to 1.8 kg of carbon dioxide. A significant advantage of algae as biomass feedstocks over first- and second-generation biofuels is their rapid growth rate, as they can double their biomass in 2–5 d [28]. The most promising advanced biofuels are derived from fourth-generation sources, which utilize genetically modified microalgae, microbes, yeast, and cyanobacteria as feedstocks [16]. Currently, significant advances have been made in genetic editing techniques and metabolic engineering aimed at developing excellent microalgae with high photosynthetic efficiency, resistance to disease, and high lipid content [31–34]. Fourth-generation biofuels offer higher productivity, increased CO_2 absorption capacity, and the potential for carbon-negative energy production through genetically engineered microorganisms compared with the lower generations.

Regarding chemical composition, oxygenated biofuels primarily comprise alcohols, fatty acid methyl and ethyl esters, ethers, and ketones. Fig. 1 illustrates the main pathways of obtaining them from biomass. Methanol can be synthesized from syngas derived from biomass, while the fermentation of sugars and cellulose can produce C_2–C_3 alcohols [35]. Methyl and ethyl esters of fatty acids, which are produced by transesterifying vegetable oils or animal fats with methanol or ethanol, respectively [35], are the main components of biodiesel. Ethers can be produced through various catalytic processes, such as direct etherification of alcohols, reductive etherification of alcohols with aldehydes or ketones, and etherification of olefins with alcohols, using heterogeneous catalysts to achieve high selectivity and yield [36]. Lignocellulose, as the second-generation biofuel feedstock with the highest commercial application potential, can undergo various processes, including pretreatment, hydrolysis, fermentation, detoxification, and distillation to produce diverse biofuels and platform compounds, including alcohols, ketones, acids, furans, and aromatic compounds [37]. Furthermore, ketones can also be indirectly synthesized from lactic acid and acetone–butanol–ethanol (ABE) fermentation products derived from biomass [38,39]. It is noteworthy that carbonates, as chemical synthesis products of alcohols, can also be indirectly derived from biomass [40,41]. Due to their extensive application in lithium-ion battery (LIB) electrolytes, carbonates have drawn significant attention in recent years [42–44].

Combustion is a significant process of energy utilization. The combustion process is a complex physicochemical phenomenon characterized by the coupling of chemical reactions with heat and mass transfer. The investigation of combustion kinetics aims to clarify the context of these reactions, from fuel consumption to the combustion intermediates and eventually products, and to provide a scientific explanation for macroscopic combustion phenomena at the microscopic molecular level. An effective kinetic model not only can elucidate the underlying causes of existing combustion phenomena, such as ignition delay time, but it can also be utilized to simulate and predict combustion parameters under unknown conditions, thereby guiding the design of burners and the control of pollutants [45].

Compared to conventional hydrocarbon fuels, oxygenated biofuels have raised new scientific challenges in combustion kinetics, particularly concerning: ① the influence of operating conditions, ② the effects of oxygenated functional groups, and ③ the interactions between oxygenates and hydrocarbons. While the combustion kinetics of certain simple biofuels such as ethanol [46–48] have been extensively studied since the early 1900s, more complex oxygenated compounds present ongoing research questions. This review begins by presenting fundamental concepts and research methodologies in combustion kinetics. It then offers a comprehensive summary of studies from the past decade on the combustion behavior of various biofuels, highlighting—through selected examples—how oxygenated functional groups influence reaction pathways and combustion characteristics. It should be noted that, although small-molecule hydrocarbon fuels derived from biomass, such as syngas [49] and biomethane [50], represent related alternatives, their kinetic networks are relatively well-established and straightforward. Therefore, they will not be discussed in detail here.

2. Combustion kinetics

Combustion kinetic models, consisting of a set of reactions and species that describe the actual reaction path, can offer valuable chemical insights into the underlying chemistry of the combustion process [51]. This precies description of actual chemical processes facilitates enhancements in combustor efficiency, significant reductions in pollutant discharge, and advancements in combustion technology.

2.1. Basic concept of kinetic mechanism

A complete kinetic model consists of thermodynamic data and transport parameters, as well as elementary chemical reactions

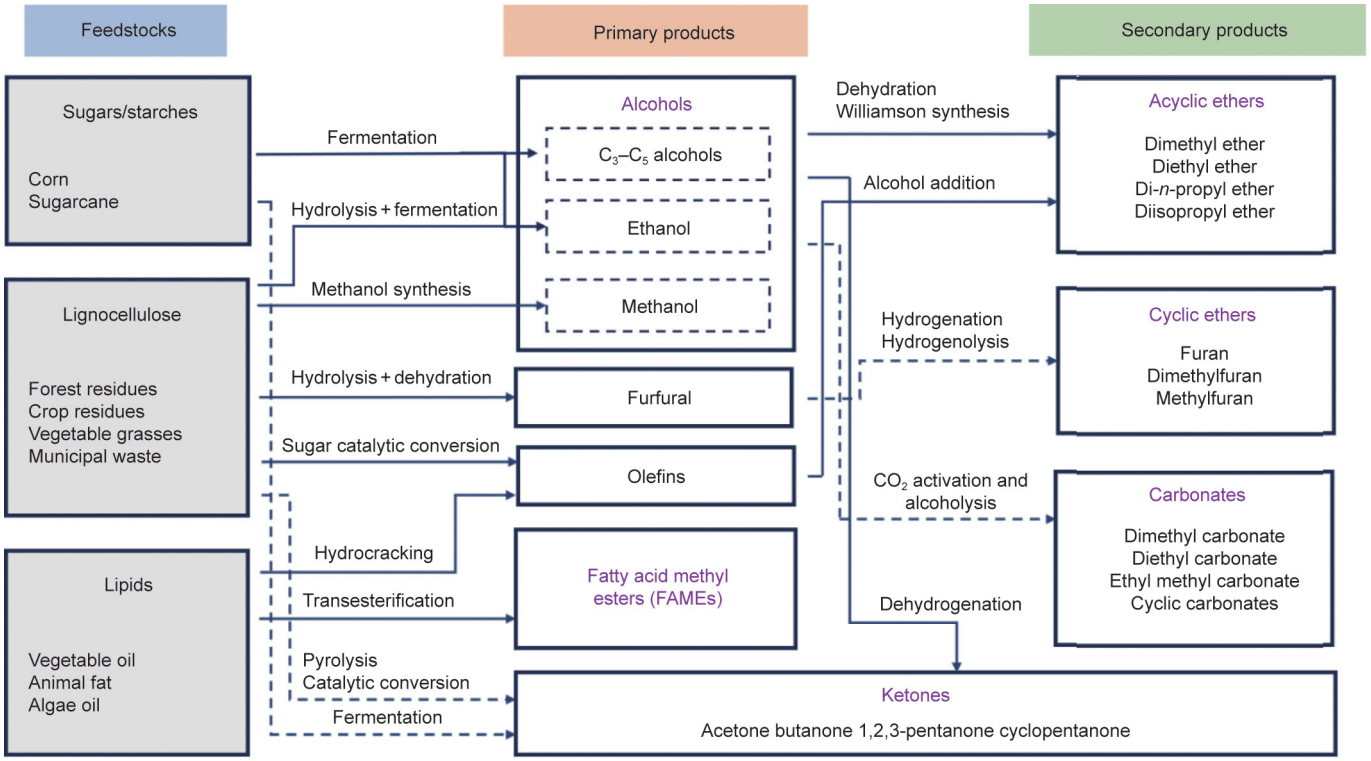

Fig. 1. Pathways to obtain oxygenated biofuels including primary products and secondary products from biomass.

with associated rate constants, which can be written in Arrhenius form [52]. The reverse rate of the elementary reaction can be derived from the relation $k_r = k_f/K_P$, where K_P is the equilibrium constant of the reaction, while k_f and k_r are the rate coefficients for the forward and reverse reactions respectively. For elementary reactions with pressure dependence (e.g., unimolecular fuel decomposition), the rate constants can be expressed using the TORE [53] or pressure–logarithmic interpolation formalism (PLOG). The temperature-dependent thermochemical properties of the species, specifically enthalpy, entropy, and heat capacities, can be represented by thermodynamic data, usually in the form of "National Aeronautics and Space Administration (NASA) polynomials" [54]. To use chemical mechanisms for simulating reactions in practical devices, it is necessary to develop the numerical model. There are several programs that are commonly used in simulating chemically reacting systems, such as Chemkin [55], Cantera [56], and OpenSMOKE [57]. These computational models address a set of differential equations that necessitate initial conditions derived from the experiments.

A comprehensive mechanism consists of numerous sub-mechanisms, with the species of these sub-mechanisms interconnected through chemical reactions. One of the most important characteristics of kinetic mechanisms is their hierarchical structure, which means that the mechanism of the large species is built upon the sub-mechanisms involving smaller species [51]. Fig. 2 [58] shows a diagram of this scheme. Currently, the widely accepted method for developing fuel kinetic mechanisms involves adding the target fuel sub-mechanism, which requires construction or further optimization, into the extensively validated C_0–C_4 core mechanism. To date, various core mechanisms have been developed and are available on the internet, such as Gas Research Institute Mechanism (GRI-Mech) [59], University of Southern California Mechanism Version II (USC Mech II) [60], foundational fuel chemistry model (FFCM) [61], National University of Ireland Galway Mechanism version 1.1 (NUIGMech1.1) [62], and AramcoMech [63–65]. Among them, NUIGMech1.1 [62] and AramcoMech [63] incorporate detailed mechanisms for the oxidation of common C_1–C_4 oxygenated fuels, encompassing alcohols, ethers, ketones, esters, and aldehydes. And AramocMech [63] has been extensively validated against experimental data for small oxygenated fuels such as methanol, ethanol, dimethyl ether (DME), and acetone across a broad temperature range. The most recently updated core mechanism is FFCM 2.0 [61], which contains C_1–C_2 alcohols and aldehydes, as well as acetone. It mainly focuses on high-temperature combustion conditions of oxygenate fuels. The elementary reactions within the fuel sub-mechanism can be categorized into distinct reaction classes [51,66,67]. These reactions, which predominate in fuel consumption, vary across different temperature ranges. Consequently, they can be classified into high-temperature and low-temperature reaction classes [68–70]. There are different rules for determining the rate constants of different reaction classes, which are progressively being refined, especially for alkanes [68,71–74]. It is noteworthy that, in recent years, quantitative calculations have increasingly contributed to determining the reaction rate constants. Moreover, the actual performance of a mechanism is often assessed against experimental results, and usually, some degree of optimization is necessary [58].

2.2. Combustion kinetics experiments and diagnostics

To thoroughly investigate the intricate kinetic reaction networks, the actual engineering environment is unsuitable due to its complex structure and flow characteristics. The experimental conditions governing combustion kinetic investigations usually involve temperature (T), pressure (P), and equivalence ratio (ϕ). Experimental devices widely adopted in research include shock tubes [75–77], rapid compression machines (RCMs) [78–80], jet-stirred reactors (JSRs) [81], plug-flow reactors (PFRs) [82], and laminar premixed flame or counterflow flame reactors [83,84], which have been subject to decades of updates and optimizations. Fig. 3

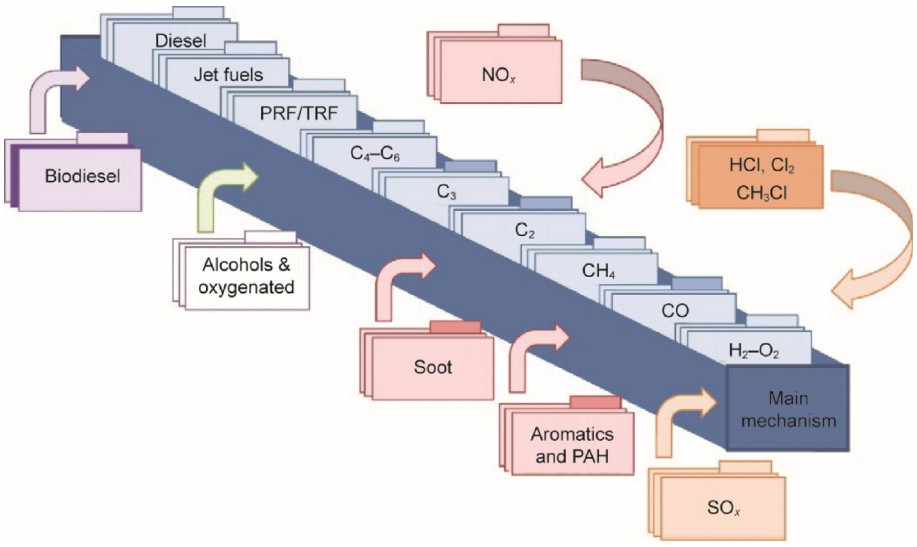

Fig. 2. Schematic diagram showing the hierarchical structure of the combustion kinetic mechanism. PAH: polycyclic aromatic hydrocarbon; PRF: primary reference fuel; TRF: technology research fuel. Reproduced from Ref. [58] with permission.

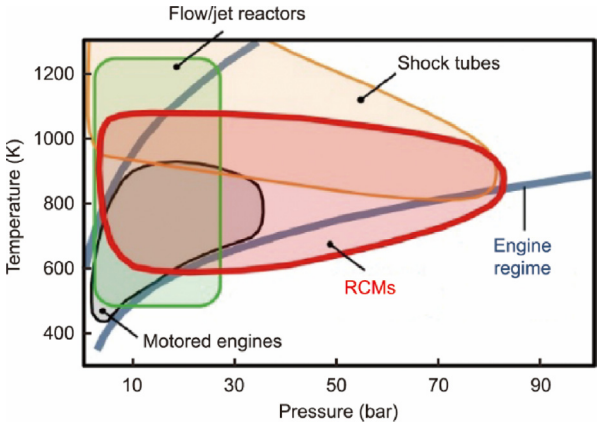

Fig. 3. Typical experimental conditions of several combustion reactors. Reproduced from Ref. [85] with permission.

[85] provides a summary of the typical operational ranges for some selected combustion reactors. These instruments are designed to evaluate critical characteristics such as laminar burning velocities (LBVs) and ignition delay times (IDTs), to assess the influence of temperature and pressure on individual elementary reactions, and to examine the pyrolysis and oxidation behavior of fuels under specific conditions [45]. In recent years, the development of experimental facilities for combustion kinetics has progressed towards acquiring data with a broader range of experimental conditions and integrating with more precise diagnostic methods. For example, Zhao et al. [86] made high-pressure (above 100 bar; 1 bar = 10^5 Pa) JSR experiments possible through a novel design, while Kang et al. [87] addressed the significant axial vibration of RCM to enable molecular beam mass spectrometry sampling.

In principle, the methodologies employed for chemical analysis can similarly be applied to combustion diagnostics, with some adaptation to account for the temperature, pressure, and geometry of the species being measured. Combustion diagnostic techniques can generally be categorized into two types: non-invasive and invasive methods. The non-invasive methods avoid disrupting the reaction environment, typically based on laser diagnostics, which benefit from the laser probe's coherent properties, offering excellent spatial and temporal resolution, as well as multidimensional imaging of various quantities [88–90]. Prior to diagnosis, it is generally essential to possess a detailed understanding of cross sections, the spectral signatures, and the expected concentration range of the target species in order to appropriately configure the laser settings. Consequently, the simultaneous detection of multiple species is often challenging due to the intricate setups [45]. In contrast to non-invasive laser-based techniques, invasive methods rely on direct sampling by a probe from the reaction environment. Common techniques include mass spectrometry (MS) and chromatography (GC) [91–93], which are suitable for the diagnosis of chemical-rich systems. Among them, photoionization molecular-beam MS (PI-MBMS), using tunable vacuum ultraviolet (VUV) synchrotron radiation for photoionization (PI) [92], is especially effective for exploring chemical pathways in intricate reaction systems due to its ability to identify substances through mass and PI efficiency (PIE) spectra [94]. Mass spectrometric analysis does not require extensive prior knowledge about the target species, and it also facilitates the detection of radicals or unstable intermediates [95,96].

2.3. Uncertainty quantification (UQ) and optimization of kinetic models

In comparing experimental data sets with simulation results, it is essential to assess the uncertainties inherent in both. Inevitably, a large number of thermodynamic parameters and rate coefficients that vary with temperature and possibly pressure will lead to uncertainties during the application process of kinetic models. A significant challenge in evaluating these model uncertainties is determining how the uncertainty ranges of individual parameters contribute to the overall uncertainty. This is often challenging since these parameters are not independent of one another [97]. Systematic quantification of uncertainties and the refinement of models through mathematical techniques have become an active field of research [98–101]. The most impactful advancement in combustion chemistry uncertainty analysis was Michael Frenklach's pioneering systematic framework for kinetic parameter uncertainties [102]. Sheen and Wang [103] devised a method for quantifying and minimizing uncertainty through polynomial chaos expansion (MUM-PCE) and advanced its use by creating the software "mumpce_py" [102]. Nagy et al. [104] and Nagy and Turányi [105] introduced a technique for assessing the

uncertainties associated with correlated Arrhenius parameters, and also conducted UQ and optimization on several existing models [99,106,107]. Global or local sensitivity analysis (SA) also plays a significant role in UQ and model optimization. Based on this, graphical user interface-high dimensional model representation (GUI-HDMR), a software tool for SA, was developed by Tomlin [108] and Ziehn and Tomlin [109].

By quantifying uncertainties and investigating their propagation, one can more effectively identify targets for experiments and model enhancements, thereby facilitating mechanism optimization and uncertainty minimization. Developing a good experimental design approach is effective to minimize uncertainty; several frameworks for experimental design have been proposed [110–113]. It is worth noting that some experimental designs often depend on data from the posterior distributions of model parameters or the results of constrained optimization to determine the most suitable experiments for optimizing the model, which can be quite time-consuming considering the computation of posterior distributions for massive potential experimental conditions [114]. Fig. 4 [114] illustrates the workflow of OptEx, a framework designed for UQ and experimental design. Within this framework, an artificial neural network (ANN) serves as a surrogate model to perform UQ and global SA. These techniques assess the probability distribution of model predictions and identify the primary sources of uncertainty, respectively. Notably, sensitivity entropy and surrogate model similarity can be derived from global sensitivity indices, facilitating informative experimental design and data categorization. Subsequently, using the available datasets, the model can be refined through Bayesian inference.

3. Kinetic research of oxygenated components of biofuels

3.1. Alcohols

The kinetics of alcohols with short carbon chains, especially methanol and ethanol, have been extensively studied since the previous century [46,47,115–119]. Despite the development of many kinetic models, accurately predicting combustion characteristics across a wide range of experimental conditions remains challenges [120]. Fig. 5(a) [59,63,121–124] compares the measured and predicted LBV of methanol. Notably, the predictive models show significant discrepancies under fuel-rich conditions, where the deviations are particularly pronounced. Fig. 5(b) illustrates the results of sensitivity analysis performed by Zhang et al [121]. The results indicate that under highly fuel-rich conditions, the reduced flame temperature enhances the dominance of reactions involving HO_2 radicals (e.g., $CH_3OH + HO_2 = CH_2OH + H_2O_2$ and $CH_2OH + O_2 = CH_2O + HO_2$). Thus, continued research efforts over the past decade have further investigated these small molecular alcohols, yielding new experimental data. Much of this recent work has aimed to broaden the range of experimental conditions—such as high-pressure environments and low-temperature regimes achieved via additives such as DME [125] and ozone [126]—while also diversifying the types of data collected, including flame properties [121] and time-resolved species concentration profiles [127–129]. In terms of reaction mechanisms, recent studies have focused more on optimizing parameters for key elementary reactions—such as $CH_2OH + O_2 = CH_2O + HO_2$ [121] and the branching ratios of H-abstraction from ethanol by OH radicals [127]—rather than developing entirely new models. These kinetic parameters are often highly constrained by experimental data obtained under specific conditions. Notably, neither methanol nor ethanol oxidation exhibits negative temperature coefficient (NTC) behavior. Additionally, advances in UQ have enabled more systematic model optimization [106,114,130,131]. For instance, Zhou et al. [114] applied a framework they developed, OptEx, to quantify uncertainties in the methanol model proposed by Zhang et al. [121] and to identify key sources of these uncertainties. Their analysis revealed that the IDT is highly sensitive to two critical parameters across all experimental conditions: the rate constant of H_2O_2 decomposition and that of H-atom abstraction from methanol by HO_2 radicals. Consequently, targeted experimental measurements under specific conditions can significantly improve the accuracy of model predictions over a wide range of scenarios.

We next note that methanol and ethanol suffer from drawbacks such as low energy density, hygroscopicity, and high corrosiveness.

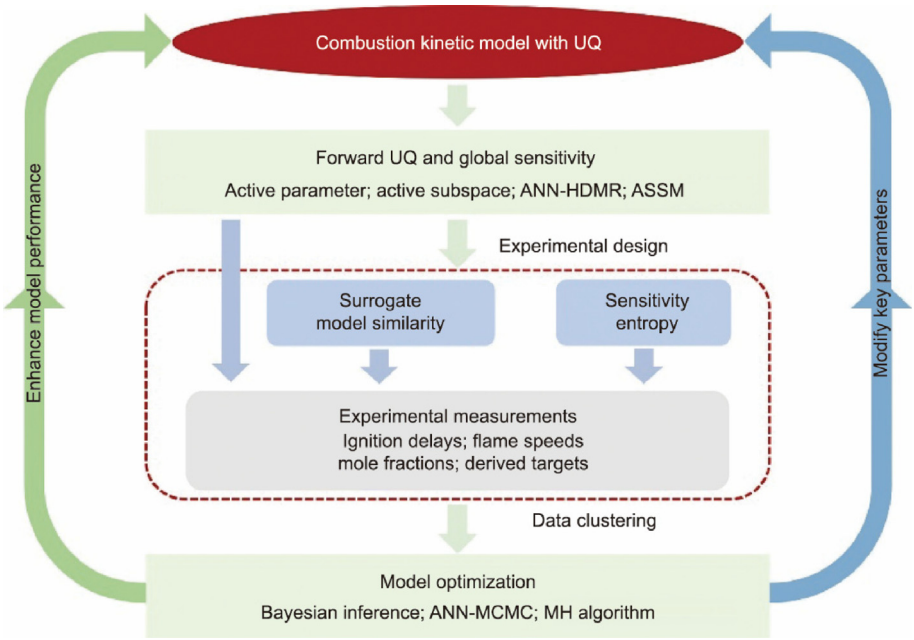

Fig. 4. Schematic of OptEx. ASSM: active subspace based surrogate model; MCMC: Markov chain Monte Carlo; MH: Metropolis–Hastings. Reproduced from Ref. [114] with permission.

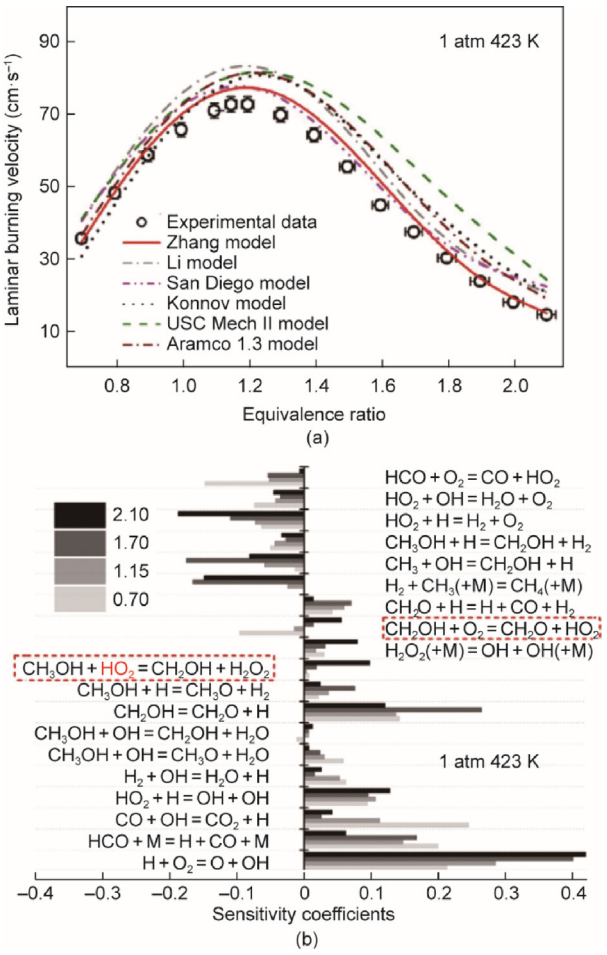

Fig. 5. (a) Measured and predicted LBV of methanol at 1 atm and 423 K. Symbols are experimental data [121] and lines are the simulation results of previous models [59,63,121–124]. (b) Results of sensitivity analysis of methanol LBV at 1 atm, 423 K and different equivalence ratio. Reproduced from Ref. [121] with permission.

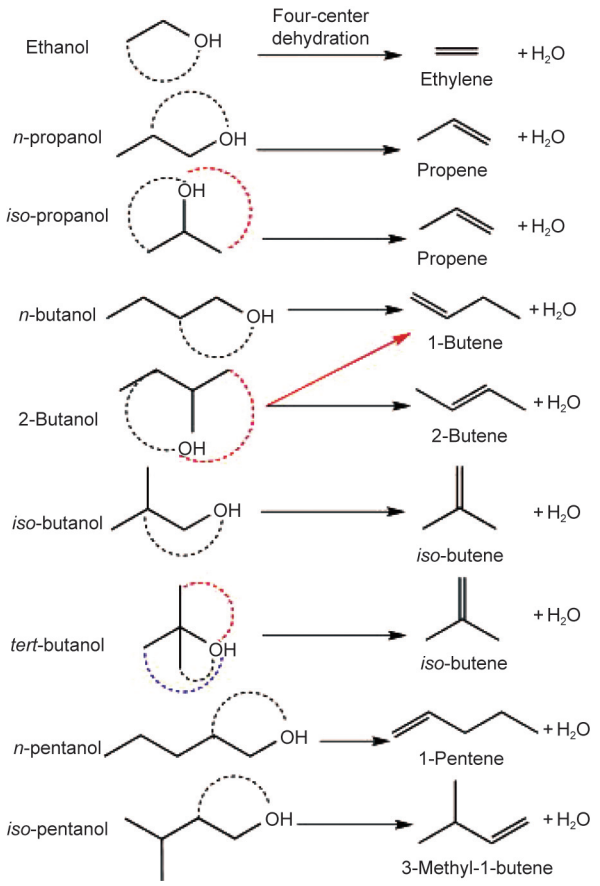

Fig. 6. Schematic diagram of the dehydration reactions of alcohols. The dotted line denotes the four-center transition state that oxygen atoms are inclined to form. There are two dehydration products of 2-butanol: 1-butene and 2-butene. Reproduced from Ref. [120] with permission.

These limitations have spurred growing interest in alcohols with longer carbon chains, particularly those spanning C_3–C_5 [132]. Among C_3 alcohols, two structural isomers exist: *n*-propanol and *i*-propanol. A variety of experimental techniques have been employed to measure their IDTs, LBVs, and species concentration profiles during oxidation [132–135]. These studies reveal that the location of the hydroxyl group significantly influences oxidation characteristics. Specifically, *n*-propanol demonstrates higher reactivity than *i*-propanol, manifesting as shorter ignition delays and higher burning velocities. The linear structure of *n*-propanol facilitates the formation of active radicals such as formyl, vinyl, and ethyl, which promote H-atom production and enhance overall reactivity. In contrast, the branched structure of *i*-propanol favors the generation of more stable radicals like CH_3 and allyl, thereby inhibiting oxidation [135]. Across all alcohols, the water elimination reaction represents a key unimolecular pathway, proceeding via a four-center transition state that involves β H atoms and the hydroxyl oxygen atom, as illustrated in Fig. 6 [120]. This reaction yields an alkene and water, and the stability of the resulting alkene influences the overall reactivity of the parent alcohol. Experimental approaches have been instrumental in quantifying reaction rates across different alcohols, as summarized in Ref. [120].

Alcohols with longer carbon chains, such as butanol and pentanol, offer higher energy density and reduced polarity compared to shorter-chain counterparts, making them promising candidates as engine fuels or additives to hydrocarbon fuels [136]. These compounds can be produced via biological routes, including glucose biosynthesis using *Escherichia coli* [137] and natural microbial fermentation facilitated by engineered microorganisms [138]. In 2012, Sarathy et al. [139] developed a detailed kinetic model encompassing all four butanol isomers (1-, 2-, *iso*-, and *tert*-butanol), which incorporated both high- and low-temperature reaction pathways. The model was validated against experimental data from premixed flames, shock tubes, and JSRs, helping to clarify dominant reaction pathways and the impact of molecular structure on combustion behavior. For pentanol isomers, Togbé et al. [140] proposed the first kinetic model for 1-pentanol, though it omitted low-temperature chemistry. This was later addressed by Heufer et al. [141], who introduced a more comprehensive model for 1-pentanol that included low-temperature reaction pathways. Köhler et al. [142] developed models for all three straight-chain pentanol isomers, still without low-temperature kinetics. Subsequently, Chatterjee et al. [143] established comprehensive kinetic models for low-temperature oxidation of 2- and 3-pentanol, enhancing model accuracy through RCM experiments. Notably, among the straight-chain pentanol isomers, low-temperature reactivity follows the order: 1-pentanol shows the highest reactivity, followed by 2-pentanol, and then 3-pentanol. Fig. 7 [143] presents a simplified reaction pathway analysis that helps clarify the low reactivity of 3-pentanol. Upon H-atom abstraction, 3-pentanol forms three distinct fuel radicals: α, β, and γ. Among these, only the γ radical can further react to form $\cdot O_2QOOH$ radicals and ketohydroperoxides (KHP), which are essential for chain branching at low temperatures [143]. Consequently, the low-temperature reac-

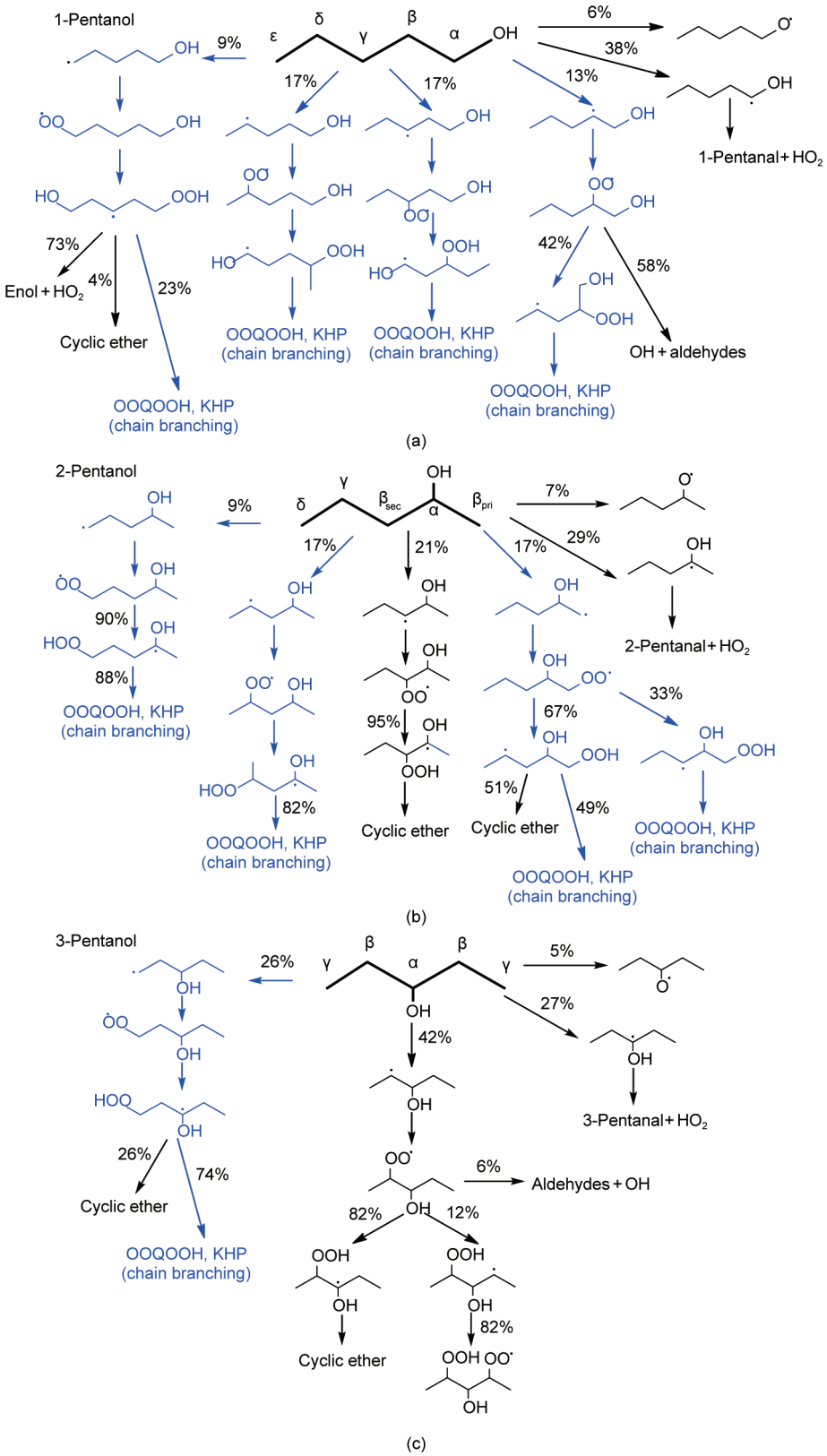

Fig. 7. Simplified reaction pathways of fuel radicals produced by H-atom abstraction reaction for different pentanol isomers: (a) 1-pentanol, (b) 2-pentanol, and (c) 3-pentanol. The blue reaction pathway identifies the chain-branching reaction. The fluxes of each pathway are derived from Ref. [143].

tivity of 3-pentanol is primarily governed by γ-radical chemistry, contrasting with other pentanol isomers that exhibit more extensive chain-branching pathways. According to the reaction pathway analysis by Chatterjee et al. [143], approximately 42% of 1-pentanol molecules undergo H-abstraction at specific sites followed by chain branching, promoting OH radical accumulation

and enhancing reactivity. In comparison, only 33% of 2-pentanol molecules follow similar pathways, explaining its intermediate reactivity relative to 1- and 3-pentanol. This systematic variation in radical branching efficiency accounts for the observed reactivity trend among the pentanol isomers. Table 1 [121,125–127,133–136,139,142,144–150] summarizes key recent studies on alcohol combustion kinetics (C_1–C_5) for reference.

Despite considerable research on alcohols, significant knowledge gaps remain even for small alcohols such as methanol and ethanol. For methanol, quantitative species profiles in high pressure flame environments are still scarce compared to data from reactor experiments [120]. Meanwhile, most ethanol models do not adequately address low-temperature kinetics (below 800 K), despite evidence confirming its reactivity in this regime [151]. Although the combustion kinetics of methanol and ethanol have been widely studied, achieving accurate model predictions across a broad range of conditions remains a challenge. This requires improved UQ and systematic analysis of error sources. The presence of the hydroxyl group also significantly influences bond dissociation energies: α C–H bonds are weakened, whereas β C–H bonds are slightly strengthened compared to those in alkanes. Consequently, key reaction rate constants—particularly for dominant pathways such as H-atom abstraction by HO_2 radicals under low-temperature conditions—still lack sufficient theoretical or experimental determination. Moreover, sub-mechanisms of critical intermediates like enols and aldehydes are not yet well established, leading to inaccuracies in predicting global reactivity and intermediate species concentrations. [133,144,145].

Table 1
Major detailed combustion kinetic models of alcohols (C_1–C_5) in recent years.

Alcohol	Conditions of validation	Reference of chemical kinetic models
Methanol	Premixed laminar flames (P = 0.04 atm, ϕ = 1.0)	[121]
	LBV in spherical combustion vessel (P = 1–10 atm, ϕ = 0.7–2.1)	
Ethanol	Laminar flow reactor (T = 600–900 K, P = 50 bar, ϕ = 0.1, 1.0, and 43)	[146]
	Shock tube and RCM (T = 650–1250 K, P = 20–40 atm, ϕ = 0.5–2.0)	[125]
	RCM (T = 769–1036 K, P = 15, 25 bar, ϕ =1.0)	[126]
	Shock tube (T = 1135–1759 K, P = 1.51–15.50 atm, ϕ = 0.5, 1.0)	[127]
Propanol	LBV in cylindrical combustion vessel (P = 1–10 atm, ϕ = 0.6–1.5)	*n*-Propanol and *i*-propanol [135]
	Shock tube (T = 1341–2073 K, P = 1.2–1.4 atm, ϕ = 0.5, 1.0, and 2.0)	*i*-Propanol [134]
	Laminar flow reactor (T = 700–1000 K, P = 20 bar, ϕ = 0.25)	*n*-Propanol and *i*-propanol [133]
Butanol	LBV in counterflow configuration (P = 1 atm, ϕ = 0.7–1.5)	1-, 2-, *iso*-, and *tert*-butanol [139]
	Premixed laminar flames (P = 0.04 bar, ϕ = 1.7)	
	RCM (T = 725–855 K, P = 15 bar, ϕ = 1.0)	
	Shock tube (T = 1050–1600 K, P = 1.5–43 atm, ϕ = 0.5, 1.0)	
	JSR (T = 770–1250 K, P = 10 atm, ϕ = 1.0)	
	RCM (T = 800–950 K, P = 15 and 30 bar, ϕ = 0.5, 1.0)	*iso*-butanol [147]
	JSR (T = 400–800 K, P = 1 atm, ϕ = 0.5)	*n*-Butanol [145]
Pentanol	Premixed laminar flames (P = 0.02 bar, ϕ = 1.5)	1-, 2-, and 3-Pentanol [142]
	LBV in spherical combustion vessel (P = 1 bar, ϕ = 0.7–1.5)	1-Pentanol and *iso*-pentanol [148]
	JSR (T = 730–1180 K, P = 10 atm, ϕ = 0.35–4)	3-Pentanol [144]
	Shock tube (T = 1000–1470 K, P = 20 and 40 bar, ϕ = 0.5, 1.0, and 2.0)	
	Shock tube and RCM (T = 690–1175 K, P = 20 and 40 bar, ϕ = 0.5–2.0)	Cyclopentanol [149]
	LBV in spherical combustion vessel (P = 1–5 bar, ϕ = 0.8–1.3)	
	JSR (T = 550–1100 K, P = 1.07 bar, ϕ = 0.5, 1.0, and 2.0)	*n*-C_3–C_6 alcohols [150]
	RCM (T = 704–935 K, P = 10 and 30 bar, ϕ = 1.0)	
	Shock tube (T = 920–1450 K, P = 6, 10, and 20 bar, ϕ = 0.5, 1.0, and 1.5)	3-Pentanol [136]

1 atm = 1.01325 bar = 1.01325 Pa.

3.2. Fatty acid methyl esters (FAMEs)

Biodiesel is widely regarded as one of the most economically viable biofuels and a promising alternative to fossil diesel, capable of partially or fully replacing it. It consists of a complex mixture of saturated and unsaturated methyl esters with carbon chains ranging from C_{14} to C_{24} [152]. The composition of FAMEs in biodiesel varies considerably depending on the feedstock source, presenting considerable challenges for the development of accurate kinetic models. As a result, a surrogate fuel approach has been adopted, wherein a single methyl ester is selected to represent the combustion behavior of real biodiesel [153]. Methyl esters commonly employed as surrogate fuels comprise both saturated species (such as methyl butanoate, methyl decanoate, methyl palmitate, and methyl stearate) and unsaturated esters (including methyl oleate, methyl linoleate, and methyl linolenate). Among these, methyl palmitate, stearate, oleate, linoleate, and linolenate are major constituents of soybean and rapeseed biodiesels, all featuring long alkyl chains [154]. Fig. 8 illustrates the chemical structures of these key surrogate compounds. Compared to saturated esters, the presence of carbon–carbon double bonds in unsaturated esters significantly influences their combustion behavior, particularly under low-temperature conditions. Specifically, the allylic sites adjacent to double bonds lower the energy barrier for H-atom abstraction, promoting rapid consumption of reactive radicals in the early stages of oxidation. Subsequently, the resulting RO_2 radicals—characterized by relatively weak R–O bonds at the allylic positions—readily decompose back into fuel radicals, thereby terminating low-temperature chain propagation pathways [155]. As a result, the presence of C=C double bonds in FAMEs suppresses low-temperature oxidation activity, with the inhibitory effect becoming more pronounced as the number of double bonds increases [156].

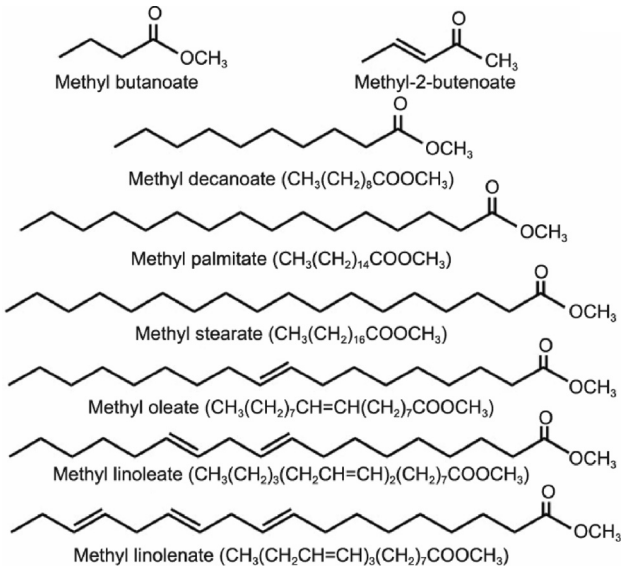

Fig. 8. Chemical structures of major biodiesel surrogate fuels.

The presence of the ester group ($CH_3OC=O$) lowers the bond dissociation energy of the C–C bond linking the ester carbon and the adjacent carbon atom. This weakening promotes cleavage of the bond in the FAME, yielding a methoxyformyl radical ($CH_3OC=O\cdot$), a key intermediate in oxygenated fuel chemistry. This radical can subsequently decompose to form CO or CO_2:

$$CH_3OC=O\cdot = CH_3\cdot + CO_2 \quad (1)$$

$$CH_3OC=O\cdot = CH_3O\cdot + CO \quad (2)$$

This process suppresses soot formation by directing carbon atoms toward the formation of small molecules, thereby inhibiting the aggregation into soot precursors [157]. Among the decomposition pathways, the route leading to CO is particularly effective in reducing soot emissions, as each oxygen atom binds a carbon atom, preventing its incorporation into larger carbonaceous species. Zhao et al. [158] calculated the potential energy surface (PES) and temperature- and pressure-dependent rate constants for these competing pathways. Their research indicates that the pathway yielding CO_2 exhibits a lower activation energy, consequently making it dominant for the decomposition of $CH_3OC=O\cdot$. A submechanism for methyl propanoate incorporating these reactions successfully predicted CO and CO_2 formation during pyrolysis in a laminar flow reactor [158]. In contrast, developing kinetic models for long-chain FAMEs is relatively straightforward in principle, as their oxidation can largely be described using rate rules derived from alkane combustion [159].

Following the progression of combustion kinetics research, methyl butanoate—the shortest-chain methyl ester surrogate—has been the most extensively studied. Fisher et al. [160] developed the first detailed mechanism in 2000, and Dooley et al. [161] later proposed a comprehensive model validated across a wide range of conditions. Subsequent work by Gaïl et al. [162] and Hakka et al. [163] further optimized the mechanism by incorporating low-temperature reaction pathways. However, despite its utility, methyl butanoate fails to capture key kinetic behaviors of long-chain methyl esters that dominate biodiesel composition, such as NTC behavior, which is absent in its oxidation [164]. In recent decades, research has shifted toward long-chain saturated and unsaturated methyl esters. Herbinet et al. [165] developed the first detailed kinetic model for methyl decanoate based on *n*-heptane oxidation principles, and Glaude et al. [166] constructed a model using EXGAS software. In 2010, Herbinet et al. [159] automatically generated a mechanism for methyl palmitate with EXGAS and validated it against JSR data. Naik et al. [167] created large-scale models for methyl stearate and methyl oleate, comprising around 3500 species and 17 000 reactions, highlighting the strong influence of double bonds on low-temperature pathways. More recently, Zhou et al. [168] and Zhou et al. [169] provided IDT data from an RCM for methyl palmitate and methyl stearate at low-to-intermediate temperatures, refining their kinetic models, respectively. They also measured IDTs for methyl oleate and methyl linoleate to assess the impact of double bonds on reactivity and autoignition, improving model predictions through SA [156]. Fig. 9 [156,168–173] compares low-temperature IDT measurements for several FAMEs with predictions from existing models, revealing significant discrepancies in ignition behavior under these conditions. Earlier reviews, such as that by Tran et al. [35], have summarized major detailed kinetic models for biodiesel surrogates and their validation status before 2012.

A paucity of experimental data and related research persists regarding authentic long-chain FAMEs present in biodiesel (e.g., methyl oleate, methyl linoleate, and methyl linoleate). Furthermore, the predictive capability of existing models, when validated against experimental results, consistently proves to be unsatisfactory (Fig. 9). The extension of the carbon chain greatly increases the complexity of kinetic models for FAMEs. For example, a detailed model representing the five main FAME components of soybean and rapeseed biodiesel includes approximately 4800 species and nearly 20 000 reactions [174]. A kinetic network of this size increases the difficulty of optimization and prohibits its use in industrial-scale simulations. As a result, research over the past decade has focused on developing simplified skeletal or lumped mechanisms with practical applicability [171,173,175,176]. Since this topic falls beyond the scope of the present review, it will not be discussed further.

3.3. Ketones

Ketones, which can be derived from lignocellulose, offer higher energy densities, improved anti-knock properties, and lower soot emissions compared to alkanes [177–179]. These advantages make them attractive as transportation fuels or fuel additives. Moreover, ketones serve as critical intermediate species in the low-temperature oxidation of alkanes [65], making their kinetic study essential for elucidating complex low-temperature reaction networks. Common ketones include acetone, butanone, 2-pentanone, and 3-pentanone. While acetone and butanone have no isomers, 2-pentanone and 3-pentanone represent the simplest straight-chain ketones exhibiting structural isomerism. Although the combustion behavior of simpler ketones such as acetone has been studied since the last century, their kinetic models have been continually refined in recent years. For instance, Hong et al. [180] significantly improved prediction accuracy by re-evaluating the dissociation reaction $CH_3COCH_3 = CH_3CO\cdot + CH_3\cdot$ based on updated experimental data (Fig. 10). A summary of recent detailed kinetic studies on ketones is provided in Table 2 [180–205].

Ignition [181,206–208] and low temperature oxidation experiments [182–184] for acetone and butanone indicate negligible low-temperature reactivity. With the extension of the carbon chain in 1- and 2-pentanone, the intramolecular hydrogen migration reaction of ROO· radicals (i.e., ROO· → ·QOOH) becomes more favorable. As a result, Fenard et al. [185] observed NTC behavior in 2-pentanone and 3-pentanone, while Kang et al. [186] identified two-stage ignition in RCM experiments, demonstrating that linear pentanones exhibit distinct low-temperature reaction pathways and reactivity. Notably, the presence of the carbonyl group in ketones influences intramolecular bond energies, specifically weakening the C–C bonds adjacent to the carbonyl group and the C–H bonds at the α-carbon positions [187,188]. This reduction in bond energy significantly promotes unimolecular decomposition and H-atom abstraction reactions at these sites. However, for intramolecular hydrogen migration reactions, the effect of the carbonyl group on the energy barrier within the transition state must also be considered. As illustrated in Fig. 11 [186,189,209], although the formation of C5KET2-OOH3-R1 involves cleavage of a C–H bond with relatively low dissociation energy, participation of the carbonyl group in the transition state leads to a higher overall energy barrier. Furthermore, unlike in alcohols, H-atom loss from the α-methylene ($-CH_2-$) or methyl ($-CH_3$) groups adjacent to the carbonyl group produces resonance-stabilized radicals [210]. When intramolecular hydrogen migration involves H-atoms from these groups, such resonance-stabilized radicals can be formed (indicated by rectangular boxes in Fig. 12 [186]). Fig. 13 [211] shows the PES for the reaction of 5-pentanone fuel radicals with O_2, revealing that the resonance-stabilized radical has the lowest relative energy among the three ·QOOH isomers. This implies a higher energy barrier for the reverse reaction to reform ROO· radicals. Consequently, although the carbonyl group slows the rate of ·QOOH formation, the low-temperature reaction network of ketones still favors the generation of these ·QOOH radicals due to

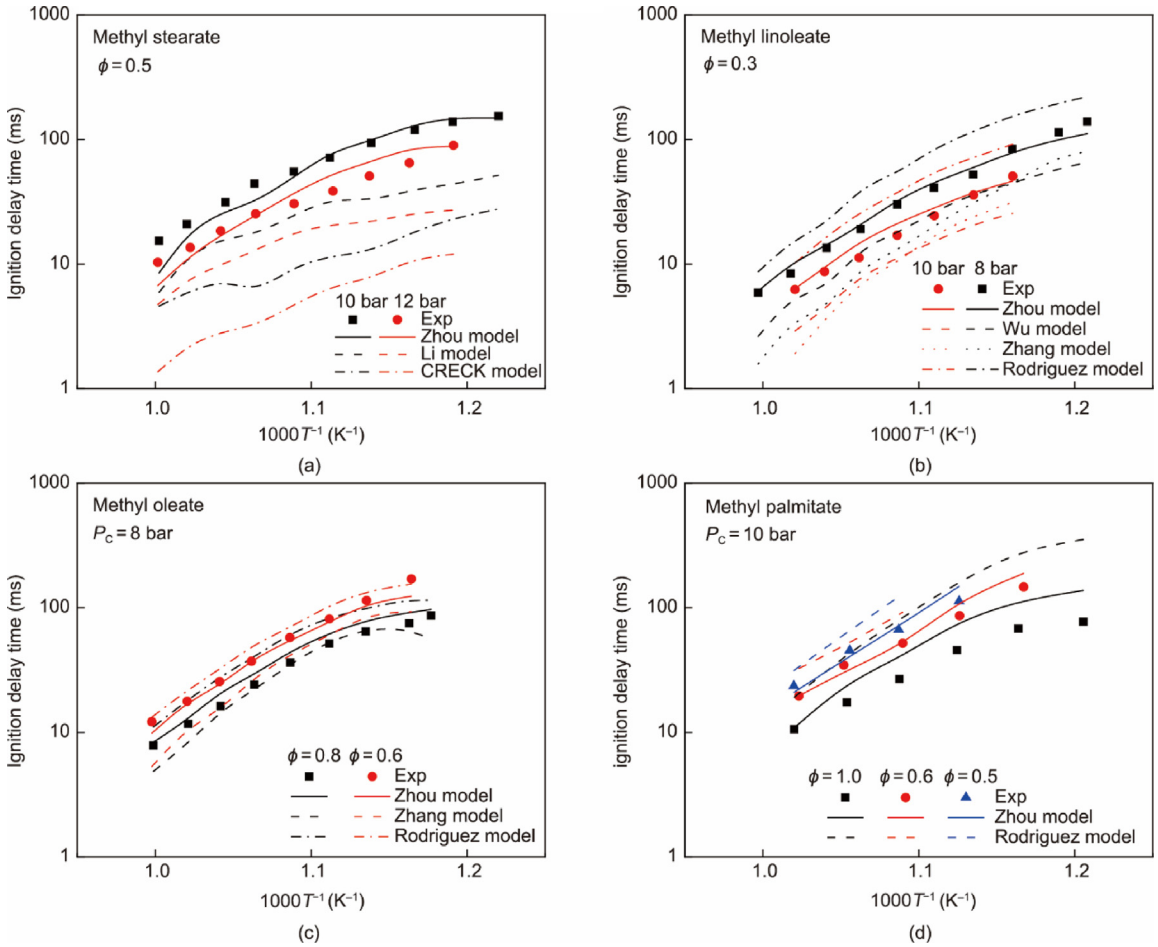

Fig. 9. Comparison of the low-temperature IDTs of various FAMEs [156,168,169] with prediction results of several published models [156,168–173]. (a) Methyl stearate at equivalence ratio of 0.5, pressure of 10 and 12 bar. (b) Methyl linoleate at equivalence ratio of 0.3, pressure of 8 and 10 bar. (c) Methyl oleate at equivalence of 0.6 and 0.8, pressure of 8 bar. (d) Methyl palmitate at equivalence of 1.0, 0.6, and 0.8, pressure of 10 bar. The calculation results are derived from Refs. [156,168,169].

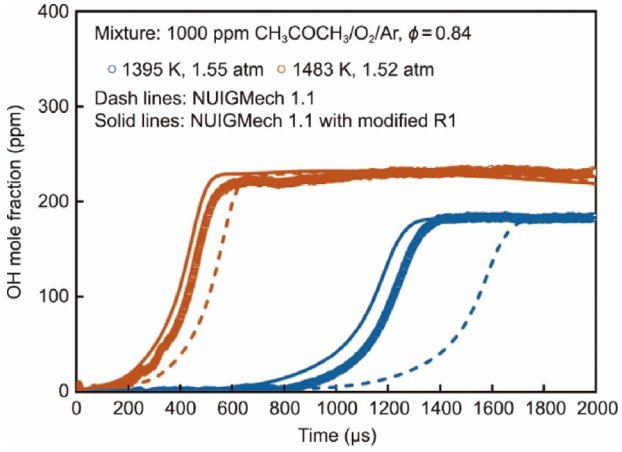

Fig. 10. OH radicals time-resolved speciation data in acetone oxidation measured in shock tube. Dash lines: NUIGMech 1.1 prediction. Solid lines: NUIGMech1.1 prediction with the revised rate constants of reaction CH_3COCH_3 = $CH_3CO\cdot$ + $CH_3\cdot$. Reproduced from Ref. [180] with permission.

the elevated reverse energy barrier—especially compared to alkanes, as depicted in Fig. 12. As a result, more fuel radicals participate in subsequent secondary oxygen addition and chain-branching reactions, leading to the formation of KHP and OH radicals, thereby enhancing low-temperature reactivity. Fig. 12 compares the reaction flux among ROO· radicals in 2-pentanone, 3-pentanone, and *n*-pentane. It can be observed that pathways yielding resonance-stabilized radicals show notably high reaction fluxes.

Regarding the oxidation of ketones at medium and high temperatures, Kang et al. [190] experimentally identified a distinctive "addition–dissociation reaction" facilitated by the carbonyl group. This reaction is proposed to proceed in two steps: first, an H or CH_3 radical adds to the carbon atom of the carbonyl group; then, the adduct dissociates into a shorter-chain aldehyde or ketone along with an alkyl radical [190]. Their developed model for pentanone oxidation incorporates this pathway using theoretically derived rate coefficients. Sun et al. [187] investigated laminar premixed flames of cyclopentanone and 3-pentanone, measuring species concentrations. They constructed a new kinetic model that showed good agreement with the experimental speciation data. Under high-temperature flame conditions (above 2000 K), the carbonyl groups in ketones are primarily released as CO, which hinders the incorporation of these carbon atoms into soot precursors. This property suggests that ketones have the potential to reduce soot emissions when used as fuel additives. Moreover, the oxygen atoms in ketones contribute only minimally to the formation of hazardous pollutants such as aldehydes and shorter-chain ketones, which arise mainly from the oxidation of hydrocarbon intermediates [187]. Minwegen et al. [212] compared IDTs measured in a shock tube and established the reactivity order of four common ketones at medium to high temperatures as follows: 3-pentanone > butanone > 2-pentanone > acetone.

Table 2
Major detailed combustion kinetic models of ketones in recent years.

Ketones	Conditions of validation	Reference of chemical kinetic models
Acetone	JSR (T = 700–1136 K, P = 1 atm, pyrolysis)	[182]
	Premixed laminar flames (P = 0.02 and 0.04 bar, ϕ = 1.0, 1.5)	[192]
	JSR (T = 600–1150 K, P = 1.07 bar, ϕ = 0.5, 1.2)	[191]
	RCM (T = 850–1100 K, P = 20 and 40 bar, ϕ = 1.0)	
	Laminar burning velocity in flat flame burner (P = 1 atm, ϕ = 0.6–1.8)	
	Time-resolved speciation in shock tube (T = 1273–1858 K, P = 1.33–1.55 atm, ϕ = 0.84)	[180]
Butanone	Premixed laminar flames (P = 0.05 bar, ϕ = 1.0)	[193]
	Shock tube and RCM (T = 850–1280 K, P = 20 and 40 bar, ϕ = 1.0)	[181]
	LBV in spherical combustion vessel (P = 1.0 and 1.5 bar, ϕ = 0.7–1.3)	
	Laminar flow reactor (T = 800–1100 K, P = 1 atm, ϕ = 1.0, 2.0)	[183]
	RCM (T = 840–945 K, P = 40 bar, ϕ = 0.5, 2.0)	
	JSR (T = 800–1200 K, P = 1 and 10 atm, ϕ = 0.5, 1.0, and 2.0)	[184]
	LBV in cylindrical combustion vessel (P = 1–10 atm, ϕ = 0.7–1.5)	[194]
Pentanone	Shock tube (T = 1250–1850 K, P = 1 atm, ϕ = 0.5–2.0)	3-Pentanone [195]
	LBV in spherical bomb (P = 1 atm, ϕ = 0.7–1.4)	
	Shock tube (T = 1277–1678 K, P = 1.6 atm, ϕ = 0.5, 1.0, and 1.5)	3-Pentanone [196]
	JSR (T = 730–1280 K, P = 1 and 10 atm, ϕ = 0.5, 1.0, and 2.0)	Cyclopentanone [197]
	Premixed laminar flames (P = 0.04 bar, ϕ = 1.5)	3-Pentanone and cyclopentanone [187]
	Premixed laminar flames (P = 0.04 bar, ϕ = 1.6)	2-Pentanone [188]
	Shock tube (T = 1150–1600 K, P = 1–5 bar, ϕ = 0.5, 1.0, and 1.5)	3-Methyl-2-butanone [198]
	RCM (T = 650–950 K, P = 20 and 40 bar, ϕ = 1.0)	3-Pentanone and 2-pentanone [185]
	Laminar flow reactor (T = 800–1050 K, P = 0.97 bar, ϕ = 0.8)	
	Flow reactor (T = 875–1428 K, P = 0.04 and 1 atm, pyrolysis)	Cyclopentanone [199]
	LBV in cylindrical combustion vessel (P = 1–10 atm, ϕ = 0.6–1.5) and in heat flux burner (P = 1 atm, ϕ = 0.6–1.5)	3-Pentanone, 2-pentanone, and 3-methyl-2-butanone [189]
	RCM (T = 895–1128 K, P = 10 and 20 bar, ϕ = 0.5, 1.0)	3-Pentanone and 2-pentanone [190]
	JSR (T = 600–1000 K, P = 0.93 bar, ϕ = 0.5)	3-Pentanone and 2-pentanone [186]
	RCM (T = 640–820 K, P = 15 and 20 bar, ϕ = 1.0)	
	LBV in heat flux burner (P = 1 atm, ϕ = 0.7–1.4)	3-Pentanone and di-isopropyl ketone
	Shock tube (T = 1125–1600 K, P = 1 and 10 bar, ϕ = 0.5, 1.0, and 1.5)	[200]
Cyclohexanone	JSR (T = 530–1220 K, P = 10 atm, ϕ = 0.5–4.0)	[201]
	Shock tube (T = 1255–1646 K, P = 2.5, 5, and 10 atm, ϕ = 0.5, 1.0, and 2.0)	[202]
Di-isopropyl ketone	Synchrotron photoionization mass spectrometry (PIMS) measurements of laser photolytic Chlorine (Cl)-initiated oxidation (T = 550–700 K, P = 0.01 bar)	[203]
	RCM (T = 591–720 K, P = 10 bar, ϕ = 1.0)	
	Shock tube (T = 1093–1630 K, P = 1–6 atm, ϕ = 0.5–2.0)	[204]
	Shock tube (T = 1100–1500 K, P = 6 and 10 atm, ϕ = 0.5, 1.0, and 2.0)	[205]

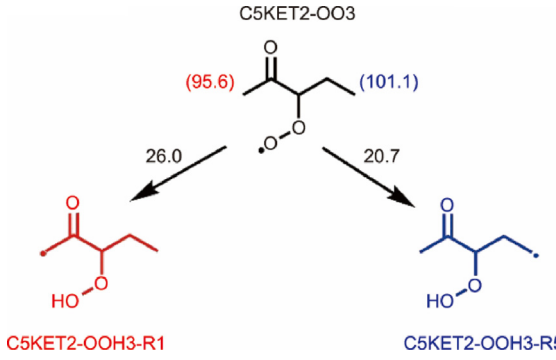

Fig. 11. The energy barriers for intramolecular hydrogen migration reactions and the bond dissociation energy of C–H bonds on various carbon atoms of the C5KET2-OO3 radical. C5KET2-OOH3-R1 and C5KET2-OOH3-R5 are two resulting products from these intramolecular hydrogen migration reactions. The barriers are obtained from calculation by Kuzhanthaivelan and Rajakumar [209] and the source of bond dissociation energy [189]. Unit: kcal·mol^{-1}. Reproduced from Ref. [186] with permission.

The construction of a comprehensive experimental database for ketone combustion remains highly valuable—even for fundamental compounds like acetone [191]. Such databases are crucial for refining kinetic models and improving predictive accuracy across a range of combustion conditions. Aldehydes, which are significant intermediate products during ketone oxidation, require deeper investigation into their formation and consumption pathways. For instance, studies on biodiesel oxidation have demonstrated that aldehydes such as formaldehyde and acetaldehyde can increase dramatically under certain conditions, underscoring the need for precise mechanistic insights. Furthermore, there is a pressing need for experimental data on special intermediates such as ketenes and vinyl ketones (e.g., methyl vinyl ketone), to accurately construct and validate their oxidation mechanisms [183,184]. The low-temperature chemistry of ketones also demands more comprehensive and detailed examination. To address these challenges, more accurate rate constants for critical reactions are essential. Advanced theoretical studies and PES calculations are also needed to uncover new reaction classes and improve existing kinetic rules.

3.4. Ethers

Chain ethers are derived from alcohols [35] and can be categorized into two distinct types: straight chain ethers and branched chain ethers. Straight chain ethers primarily consist of DME, diethyl ether (DEE), and di-*n*-propyl ether (DPE), whereas branched chain ethers include methyl tert-butyl ether (MTBE), ethyl *tert*-butyl ether (ETBE), and diisopropyl ether (DIPE). These compounds are mainly utilized as gasoline additives [213]. The presence of an ether bond significantly reduces the bond dissociation energy of the adjacent C–C and C–H bonds, thereby enhances their low-temperature reactivity in comparison to the corresponding alkanes. DME, recognized as the simplest ether, is among the most extensively studied. In 1996, Dagaut et al. [214] proposed the first detailed combustion mechanism of DME. Following numerous updates and optimizations, the current models showed satisfactory predictive performance on measured IDTs data, NTC

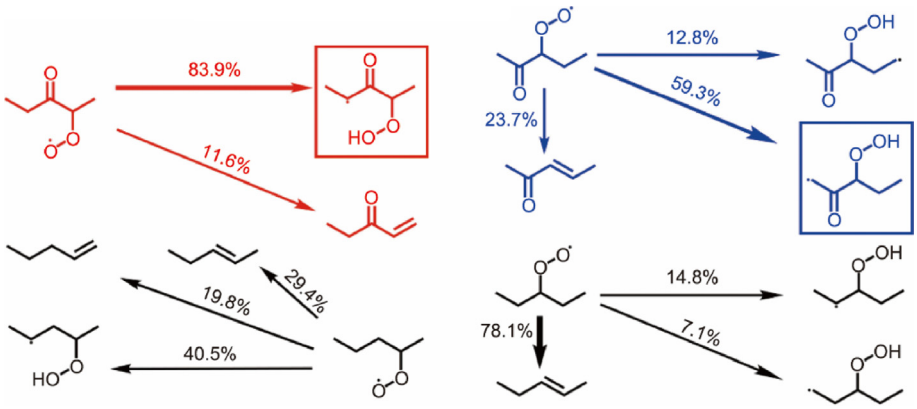

Fig. 12. The reaction flux of ROO· radicals generated in the oxidation systems of 2-pentanone (blue), 3-pentanone (red), and *n*-pentane (black) in the conditions of JSR experiments at 840 K. Resonance-stabilized radicals are identified by rectangular enclosures. Reproduced from Ref. [186] with permission.

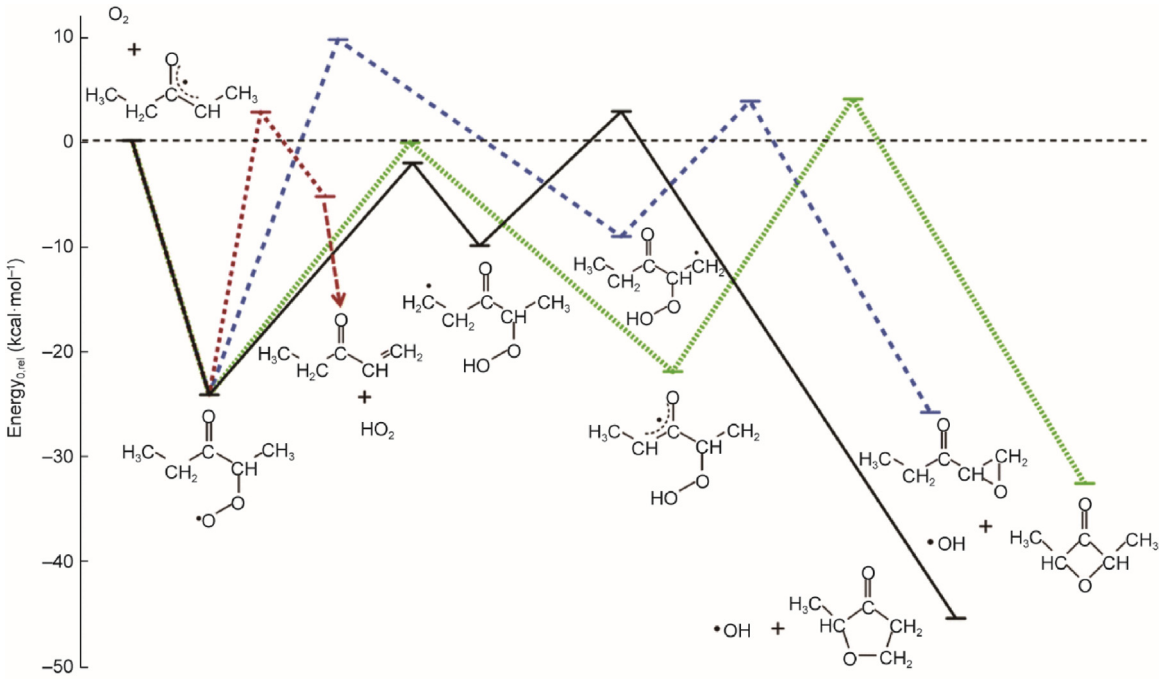

Fig. 13. PES for the reaction of the secondary diethyl ketone radical + O_2. Energies at 0 K are at the CBS-QB3 level. Reproduced from Ref. [211] with permission.

behavior, and the concentration profiles of some key intermediates such as formaldehyde and formic acid [215–217]. For long straight ethers, such as DEE [218], DPE [219], and di–*n*–butyl ether [220], an interesting phenomenon was observed, that there are two NTC zones in their oxidation. These two zones can be distinctly identified in Fig. 14(a) [218–221]. Fig. 14(b) compares the experimental results of two dipropyl ether isomers, and it can be observed that the branched ether does not exhibit NTC behavior in similar conditions. Fan et al. [219] elucidated this double NTC behavior in their oxidation investigation of DPE and Fig. 15 shows their reaction pathway analysis results. The emergence of the first NTC zone of DPE can be attributed to factors similar to those affecting alkanes, specifically the competition between the decomposition of the fuel radical and the low-temperature reaction pathway. As illustrated in Fig. 15 [219], at 530 K, fuel radicals formed from H-atom abstraction undergo a sequential reaction pathway to produce ROO· ($C_3H_7OC_3H_6OO$-A), ·QOOH (C_3OC_3-AOOH-1), ·OOQOOH (C_3OC_3-AOOH-1OO), and KHP (C_3OC_3KETA-1), ultimately resulting in the net generation of OH radicals and demonstrating the low-temperature activity of DPE. Around 590 K, an increased temperature favors the decomposition of fuel radicals, primarily producing *n*-C_3H_7 and C_2H_5CHO, which diminishes the overall reactivity and contributes to the first NTC behavior. With further increases in temperature, the concentrations of intermediates *n*-C_3H_7 and C_2H_5CHO rose rapidly, becoming predominant in the oxidation system at this stage. Due to their typically higher low-temperature activity range (around 600–700 K) compared to DPE, these species once again undergo a similar reaction competition as mentioned above, leading to the emergence of second NTC behavior. This theory also accounts for the NTC behavior observed in other ethers [219]. Fig. 16 [219,222] shows the concentration profiles of some typical intermediate species during the DPE oxidation process. Propanal exhibits the highest peak mole fraction in the low-temperature region, which is consistent with its key role in the formation of the observed double-NTC behavior. The observed substantial formation of small molecular hydrocarbons (CH_4, C_2H_4, and C_3H_6) at elevated temperatures also supports the conclusion drawn from the reaction pathway analysis. Further-

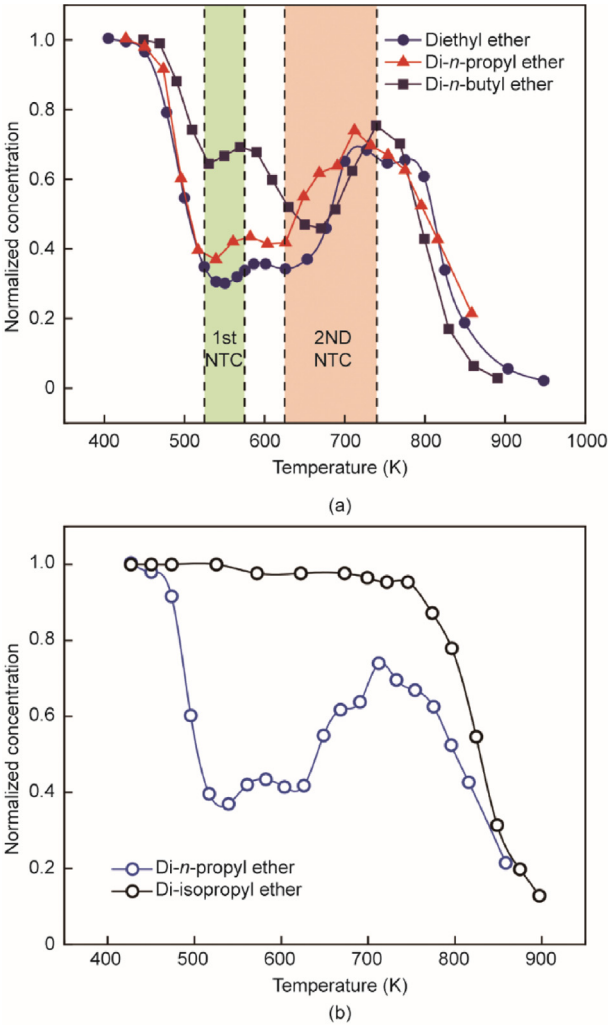

Fig. 14. (a) Experimental species profiles of different long straight ethers in JSR: DEE (ϕ = 1.0, P = 1 atm, and τ = 2 s) [218], DPE (ϕ = 1.0, P = 1 atm, and τ = 2 s) [219] and di-*n*-butyl ether (ϕ = 2.0, P = 10 atm, and τ = 700 ms) [220]. (b) Experimental species profiles of two dipropyl ether isomers in JSR at similar conditions (ϕ = 1.0, P = 1 atm, and τ = 2 s): DPE [219] and di-isopropyl ether [221]. τ represents the residence time of gas mixtures in JSR. The curves are trendlines and symbols are experimental data.

more, significant discrepancies remain between model predictions and experimental data for certain oxygenated intermediates (e.g., C_2H_3OH and CH_2CO), which provides a direction for future works. Differently, branched chain ethers do not demonstrate such significant low-temperature activity, although the presence of O atoms still facilitates the H-atom abstraction reactions and the ROO· isomerization. The primary reason is that the branched-chain structure results in a higher energy barrier for the subsequent formation of hydroperoxyalkyl peroxy radicals (·OOQOOH) and KHP, thereby diminishing the production of OH radicals [221]. Major detailed kinetic models of chain ethers proposed in recent years are summarized in Table 3 [215–237].

Cyclic ethers, derived either from fructose enzymatically produced from starch [238] or through a catalytic process from cellulosic biomass [239], have the potential to serve as valuable alternatives to fossil fuels for transportation. The reaction classes in the oxidation mechanisms of cyclic ethers are fundamentally analogous to those of cyclic alkanes. However, the reaction rate constants are subject to modification due to the presence of O atoms [35]. Furthermore, polyoxymethylene DME ($PODE_n$), characterized by its distinctive C–O alternating chain structure ($CH_3O(CH_2O)_nCH_3$), can be synthesized from methanol, DME, or formaldehyde [240]. It has been demonstrated to reduce particulate matter and soot emissions when used as a fuel additive [241], and relevant combustion kinetic studies have been constructed in recent years. Kinetic models for these mentioned fuels are also listed in Table 3.

So far, discrepancies still persist between models and experimental results at low-temperature regimes for ethers, particularly long-chain ethers. This underscores the need for a deeper understanding of the intricate chemistry involved in their oxidation process at low temperatures. The impact of ether functional groups on the low-temperature chemistry of fuels and the decomposition of oxygen-containing intermediates can serve as a starting point for further theoretical investigations. Additionally, sensitivity analyses of these models indicated that the rate constants of certain key reactions may require reevaluation to enhance model performance. These include H-atom abstraction by HO_2 and OH radicals, decomposition of ethers and KHP species.

3.5. Carbonates

In recent years, the global appetite for electric vehicles (EVs) has surged, and LIBs have become the preferred choice for energy storage in EVs. This is due to their relatively high energy density, excellent cycling performance, high operating voltage, and extended lifespan [242,243]. As the primary component of the electrolyte in LIBs, investigation of the combustion kinetics of carbonates is essential to accurately understand the thermal runaway process of batteries and to develop effective thermal management strategies. Electrolyte solvents commonly consist of mixtures of various carbonates, including linear carbonates dimethyl carbonate (DMC), diethyl carbonate (DEC), and ethyl methyl carbonate (EMC), as well as the cyclic carbonates ethylene carbonate (EC) and propylene carbonate (PC) [244]; their chemical structures are shown in Fig. 17. Since they can be synthesized from alcohols and can be indirect products of biomass [41], the kinetic investigations of carbonates are also included in this review.

In 2005, Glaude et al. [157] proposed the first detailed oxidation kinetic model of DMC. Building upon this model, Hu et al. [245] and Sun et al. [246] subsequently constructed respective high-temperature oxidation mechanisms. These mechanisms were validated using IDTs data and laminar premix flame species data, respectively. The most recent kinetic study of DMC was conducted by Yu et al. [247], who validated the existing models by the measured low-temperature ignition delay data and modified the rate constants of several crucial H-atom abstraction reactions at low temperature. Owing to the relatively weak activity of DMC at low temperatures, none of the proposed mechanisms so far contains low-temperature reaction pathways analogous to those of alkanes. At medium and low temperatures, DMC is primarily consumed through H-atom abstraction reactions to generate fuel radicals ($CH_3OC(=O)OCH_2·$), which subsequently decompose to $CH_3OC(=O)O·$ and $CH_3OC(=O)·$ radicals [247]. Notably, at high temperatures, linear carbonates are capable of undergoing a distinct unimolecular decomposition reaction known as the CO_2 elimination reaction. In this process, the C atom within the carbonate group is released as CO_2, leaving behind one O atom to form an ether [248]. Fig. 18 [249] illustrates the comparative reaction fluxes of DMC at low and high temperatures. The dominant reaction pathway at low temperatures is H-atom abstraction, leading to the formation and subsequent decomposition of fuel radicals. However, at high temperatures, CO_2 elimination becomes an increasingly important reaction. Table 4 [80,157,246,248,250] presents the rate constants and activation energies for CO_2 elimination reactions of linear carbonates, along with their corresponding literature sources. In 2015, Nakamura et al. [251] developed the first oxidation mechanism for

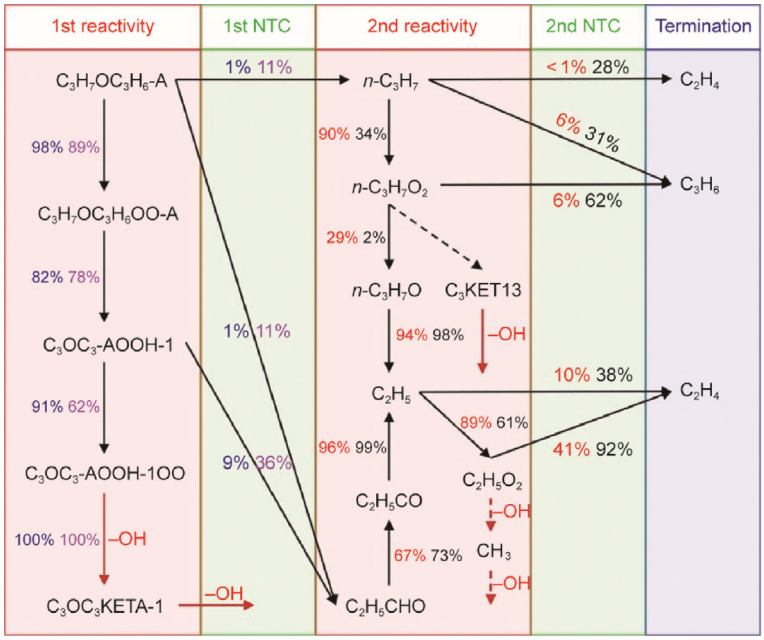

Fig. 15. Reaction pathway analysis of DPE oxidation at different temperatures. The reaction flux of DPE is derived from ROP analyses, with the figure representing the percentage of the source species consumed. Blue: 530 K; magenta: 590 K; red: 630 K; black: 730 K. Reproduced from Ref. [219] with permission.

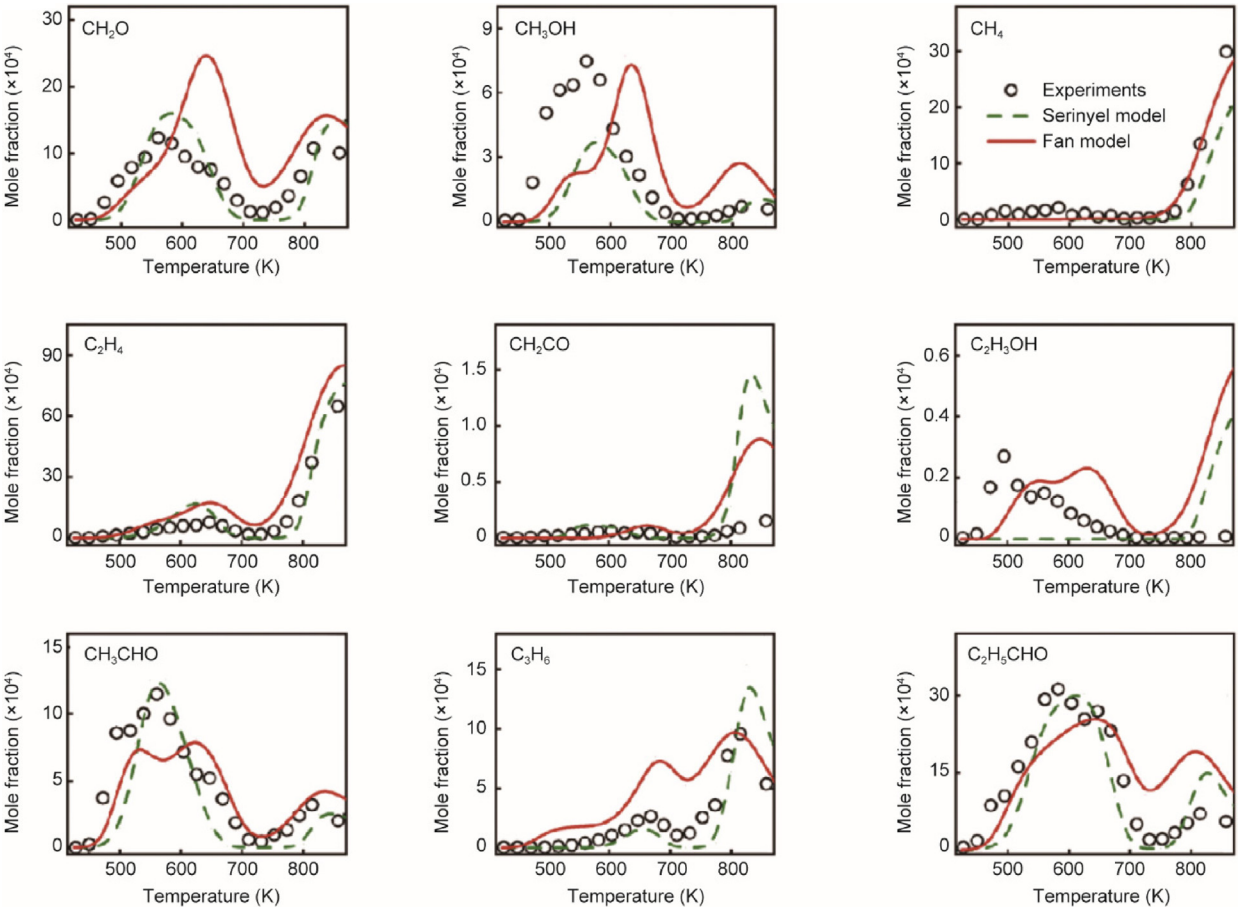

Fig. 16. Experimental and simulated typical intermediate species mole fraction profiles in the oxidation of DPE. Symbols: experimental data from Ref. [219]. Lines: simulated results through the models proposed by Refs. [219,222]. Reproduced from Ref. [219] with permission.

DEC, in which the rate constants of ROO· ⇌ ·QOOH isomerization were determined through quantitative calculation, and other low-temperature pathways and the associated parameters were obtained by analogy. The existence of these pathways could be demonstrated by the observed NTC behavior in RCM and JSR experiments [251,252]. Another significant reason for the higher activity

Table 3
Major detailed combustion kinetic models of ethers in recent years.

Ether	Conditions of validation	Reference of chemical kinetic models
DME	Shock tube and RCM (T = 600–1600 K, P = 7–41 atm, ϕ = 0.3–2.0)	[215]
	Laminar flow reactor (T = 400–1160 K, P = 1 atm, ϕ = 1.0)	[216]
	Laminar flow reactor (T = 400–1100 K, P = 1 atm, ϕ = 0.8, 1.0, and 1.2)	[217]
	Shock tube (T = 1188–1823 K, P = 1.5 and 15.5 atm, ϕ = 0.5–2.0)	[223]
Ethyl methyl ether	JSR (T = 375–850 K, P = 1 atm, ϕ = 1.0)	[224]
DEE	JSR (T = 450–1250 K, P = 1 and 10 atm, ϕ = 0.5, 1.0, and 2.0)	[225]
	JSR (T = 400–1100 K, P = 1 atm, ϕ = 1.0)	[218]
DPE	JSR (T = 470–1160 K, P = 10 atm, ϕ = 0.5–4.0)	[222]
	JSR (T = 425–850 K, P =0.93 bar, ϕ = 1.0)	[219]
	LBV in cylindrical combustion vessel (P = 1–10 atm, ϕ = 0.7–1.5)	DPE and DIPE [226]
Di-*n*-butyl ether	Laminar flow reactor (T = 485–525 K, P = 1 atm, ϕ = 0.5, 0.7, and 1.0)	[227]
	LBV in stagnation flow configuration (P = 1 atm, ϕ = 0.7–1.5)	
	JSR (T = 470–1250 K, P = 1 and 10 atm, ϕ = 0.5, 1.0, and 2.0)	[220]
	Shock tube (T = 900–1300 K, P = 20 and 40 bar, ϕ = 0.5, 1.0)	[228]
	RCM (T = 550–650 K, P = 10, 20, and 40 bar, ϕ = 0.5, 1.0)	
MTBE	Shock tube (T = 1023–1447 K, P = 3.5 and 12 atm, ϕ = 1.0)	[229]
ETBE	LBV in spherical bomb (P = 1, 3, and 5 atm, ϕ = 0.7–1.6)	[230]
DIPE	JSR (T = 525–900 K, P = 1 atm, ϕ = 1.0)	[221]
Tetrahydrofuran	LBV in heat flux burner (P = 1 atm, ϕ = 0.55–1.60)	[231]
	Shock tube (T = 1300–1700 K, P = 8.5 atm, ϕ = 0.5–2.0)	
2,5-Dimethylfuran	Shock tube (T = 1150–2010 K, P = 1.2, 4, and 16 bar, ϕ = 0.5, 1.0, and 2.0)	[232]
2-Methylfuran	Premixed laminar flames (P = 0.04 bar, ϕ = 0.8, 1.0, and 1.5)	[233]
2-Methyltetrahydrofuran	RCM (T = 640–900 K, P = 3–21 bar, ϕ = 1.0)	[234]
2,5-Dimethyltetrahydrofuran	Shock tube and RCM (T = 650–1300 K, P = 10–40 bar in ST and 10–20 bar in RCM, ϕ = 1.0)	[235]
Polyoxymethylene DME	Premixed laminar flames (P = 0.03 bar, ϕ = 1.0)	[236]
	LBV in cylindrical combustion vessel (P = 1 atm, ϕ = 0.7–1.6)	
	RCM (T = 640–865 K, P = 10, 15 bar, ϕ = 0.5, 1.0, and 1.5)	[237]

of DEC at low temperature is that DEC can decompose into ethoxyformic acid and ethylene, and a six-membered ring transition state involving an ethyl ester group was formed in this reaction:

$$C_2H_5OC(=O)OC_2H_5 = C_2H_4 + C_2H_5OC(=O)OH \quad (3)$$

The ethoxyformic acid can rapidly decompose into CO_2 and ethanol. It is noteworthy that, owing to its lower activation energy [248], this reaction becomes the dominant pathway during pyrolysis for carbonates containing ethyl groups, rather than the CO_2 elimination reaction [253].

Because of the experimental challenges caused by the extremely low saturated vapor pressure of cyclic carbonates (e.g., the saturated vapor pressure of EC is only 390 Pa at 373 K [254]), the advance of combustion kinetics in cyclic carbonates is considerably slower compared to that of linear carbonates. In 2024, Kanayama et al. [255] first developed a detailed surrogate model for LIB electrolytes, which includes the pyrolysis and oxidation of EC, DMC, EMC, and DEC. One year later, Dong et al. [256] enhanced this model by revising and adjusting the rate constants for several reactions associated with the generation and depletion of the formyl methyl radical ($\cdot CH_2CHO$) and ketene. The optimized model improved the prediction of the species data measured in JSR. The $\cdot CH_2CHO$-related and CH_2CO-related chemistry have shown significant influence on the pyrolysis and oxidation of EC. As a cyclic carbonate, EC can also undergo the CO_2 elimination reaction, yielding CO_2 and C_2H_4O isomers, including acetaldehyde (CH_3CHO), oxirane ($C_2H_4O_{1-2}$), and vinyl alcohol (C_2H_3OH). This is the main pathway for the consumption of EC in pyrolysis [257]. Furthermore, the authors have not found any pertinent studies on the combustion kinetics of PC. The major detailed kinetic models proposed recently on these carbonates are shown in Table 5 [245–249,253,255,256,258–260]. For further kinetic study of cyclic carbonates, the priority is to enrich the experimental data of oxidation and pyrolysis, particularly the species profiles of key intermediates such as C_2H_4O isomers, $\cdot CH_2CHO$, and CH_2CO, thereby further constraining the predictive performance of the existing models. Further refinement of the EC kinetic model requires particular attention to the reaction pathways responsible for acetaldehyde generation at low temperatures (< 900 K). Additionally, the reaction rate coefficients related to $\cdot CH_2CHO$ may also need to be re-evaluated [256]. In the development of a kinetic model for PC, a suitable initial step would involve the computation of the PES and branching ratios for CO_2 elimination reaction via quantum chemical methods.

4. Conclusions and perspectives

As the energy crisis exacerbated by fossil fuels intensifies, biofuels have garnered increasing attention due to their benefits, including carbon neutrality and the accessibility of raw materials. Maximizing these benefits of biofuels necessitates not only a comprehension of their physical properties but also a thorough understanding of the chemistry underlying the combustion processes. This review introduces the combustion kinetics of oxygenated fuels derived directly or indirectly from biomass, including alcohols, FAMEs, ketones, ethers, and carbonates, over the last decade. The kinetic characteristics of these oxygenated fuels, along with the corresponding detailed models proposed in recent years, are presented. Alcohols have a special unimolecular dehydration reaction with a four-center transition state, generating an alkene and water. For long-chain alcohols, the influence of the hydroxyl group's position on low-temperature activity is primarily determined by the feasibility of the low-temperature chain branching reactions of the corresponding fuel radicals, which are generated through H-abstraction reactions. Long-chain FAMEs constitute the primary fraction of biodiesel fuel. The ester group contributes to a reduction in soot formation. The reaction classes of FAMEs are fundamentally similar to those of long-chain hydrocarbons. Moreover, the degree of unsaturation in FAMEs exerts a considerable influence on their reactivity, primarily attributable to the week bond dissociation energy at the allylic sites. During the oxidation of ketones, the resonance-stabilized radicals are easily formed, which significantly impact the reaction energy barrier. This, in turn, accounts for the differences in reaction flux between ketones and hydrocarbon fuels. Additionally, a distinct double NTC

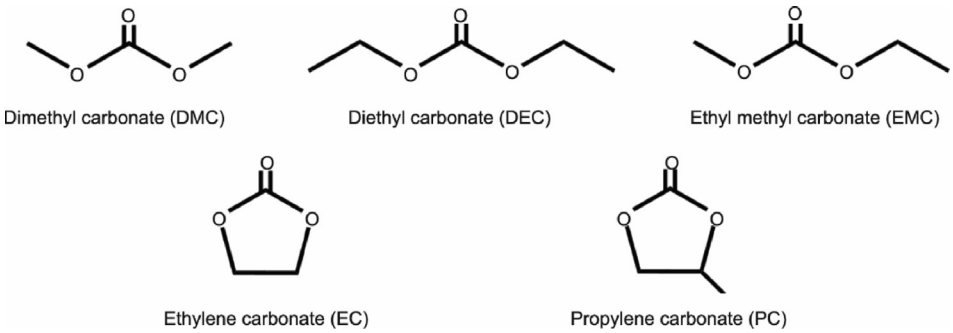

Fig. 17. Chemical structures of five carbonates in the electrolyte of LIBs.

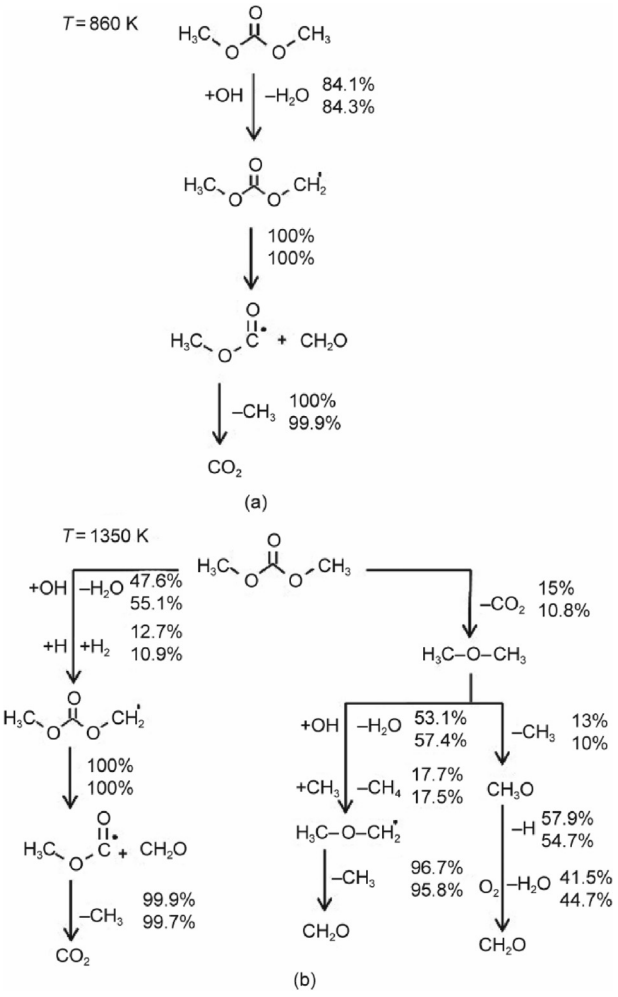

Fig. 18. Reaction pathway analysis of DMC oxidation at (a) T = 860 K and (b) T = 1350 K for P = 20 and 40 atm, ϕ = 0.5. The fuel consumption is 20%. Reproduced from Ref. [249] with permission.

behavior was observed in the oxidation of straight-chain ethers. This phenomenon is attributed to the varying low-temperature activity of fuel molecules and intermediates generated in the oxidation process. In contrast, due to the higher energy barrier for the formation of ·OOQOOH and KHP, the branched ethers do not exhibit high low-temperature activity. Carbonates, as indirect derivatives of biomass, constitute the primary components of electrolyte solvents in LIBs, and their kinetic properties have garnered significant attention in recent years. For short-chain carbonates and cyclic carbonates, the CO_2 elimination reaction represents a distinctive and significant decomposition pathway particular at high temperature. In the case of long-chain carbonates such as DEC and EMC, owing to the lower activation energy, the fuel molecules are more likely to decompose via a pathway involving the formation of a six-membered ring transition state. The kinetics of cyclic carbonates remain relatively underexplored, necessitating further experimental validation of the models.

To facilitate the extensive application of biofuels, it is significant to gain a comprehensive understanding of their fundamental combustion characteristics and to develop predictive combustion kinetic models that are applicable under practical conditions. This necessitates further requirements for future research:

Deep insights into the combustion chemistry of biofuels are predicated on experimental observations, and further experimental research involving oxidation and pyrolysis remains essential. This includes diversifying the types of fuels studied, broadening the sources of experimental data, and expanding the range of experimental conditions. Particularly, the presence of oxygen-containing functional groups significantly influences the low-temperature activity of fuels, which mean additional low-temperature experimental data for various fuels is still highly necessary. New experimental methods, such as the addition of active component like ozone, hold potential for facilitating kinetic investigations at low-temperature oxidation systems. Meanwhile. it is necessary to advance combustion diagnostic technologies to enable more precise measurement of key intermediates in the combustion process of biofuels. In combustion environments, specific intermediates, such as aldehydes generated during ketone oxidation and enones formed during cyclic carbonate oxidation, are critical for providing essential constraints during kinetic model refinement and optimization.

The presence of oxygen-containing functional groups has a substantial impact on the bond dissociation energy of molecules. Consequently, determining the reaction rate constants needs additional experimental investigations and theoretical calculations, rather than relying solely on analogies with the same reaction classes of alkanes. There is a need for elementary kinetic

Table 4
CO_2 elimination reactions of linear carbonates.

Carbonate	A^a	n^b	$E_a{}^c$	Reference
DMC	5.00×10^{11}	0.19	6.98×10^4	[157]
	1.49×10^{43}	−8.53	8.47×10^4	[246]
	2.02×10^{13}	0	3.42×10^4	[80]
DEC	3.58×10^{29}	−4.63	7.48×10^4	[248]
EMC	9.76×10^{13}	0	6.76×10^4	[250]

Rate coefficients are given as $k = AT^n e^{-E_a/RT}$, where R is the universal gas constant (1.987 cal·mol^{-1}). Units are s^{-1}, cm^3, and cal·mol^{-1}.
[a] Pre-exponential factor.
[b] Temperature exponent.
[c] Activation energy of the elementary reaction.

Table 5
Major detailed combustion kinetic models of carbonates in recent years.

Carbonate	Conditions of validation	Reference of chemical kinetic models
DMC	Shock tube (T = 1100–1600 K, P = 1.2–10 bar, ϕ = 0.5, 1.0, and 2.0)	[245]
	Premixed laminar flames (P = 0.03 and 0.04 bar, ϕ = 1.0, 1.5)	[246]
	Shock tube and RCM (T = 795–1585 K, P = 2.0, 20, and 40 atm, ϕ = 0.5, 1.0, and 2.0)	[253]
	RCM (T = 778–1102 K, P = 20 and 40 bar, ϕ = 0.5, 1.0, and 2.0)	[247]
DEC	Shock tube and RCM (T = 660–1300 K, P = 30 bar, ϕ = 0.5, 1.0, and 2.0)	[249]
	JSR (T = 500–1200 K, P = 10 atm, ϕ = 0.5, 1.0, and 2.0)	
	Premixed laminar flames (P = 0.03 bar, ϕ = 1.5)	[248]
	Shock tube (T = 1182–1406 K, P = 1 atm, ϕ = 0.5, 1.0, and 2.0)	[258]
	LBV in constant-volume vessel (P = 1 atm, ϕ = 0.79–1.38)	
EMC	Micro flow reactor (T = 700–1300 K, P = 1 atm, ϕ = 0.5, 1.0, and 1.5)	[259]
	Shock tube (T = 1175–1481 K, P = 1 atm, ϕ = 0.5, 1.0, and 2.0)	[260]
	LBV in constant-volume vessel (P = 1 atm, ϕ = 0.8–1.4)	
EC	Shock tube (T = 1228–1717 K, P = 1 atm, ϕ = 0.5, 1.0, and 2.0)	[255]
	JSR (T = 600–1150 K, P = 1 atm, ϕ = 0.5)	[256]

rate measurements for some key reactions of biofuels, including special decomposition reactions of fuels, H-atom abstraction reactions and decomposition of intermediates. H-atom abstraction reactions by HO_2 and OH radicals warrant increased research attention due to their substantial importance in the low-temperature oxidation of oxygenated fuels. Furthermore, through the application of quantum chemical calculations and theoretical research on PES, special reaction classes can be revealed and their rate parameters can be determined, such as the dehydration reactions of alcohols [261], addition-dissociation reactions of ketones [190] and CO_2 elimination reactions [246,248] of carbonates, as mentioned in this paper.

In addition to the aforementioned experimental and theoretical investigations, advanced mathematical methods leading to more reliable models are highly desired. These include new automated mechanism generation methods, experimental design based on model analysis, and physics-based artificial intelligence methodologies. Moreover, the advances of UQ and model optimization techniques can significantly enhance the predictive accuracy. Suitable and efficient methods for simplifying intricate mechanisms can substantially reduce computational costs, thereby adapting to the practical application of biofuels in energy systems.

CRediT authorship contribution statement

Xiao Liu: Writing – original draft, Methodology, Investigation, Conceptualization. **Chung K. Law:** Writing – review & editing. **Bin Yang:** Writing – review & editing, Investigation, Funding acquisition, Conceptualization.

Declaration of competing interest

The authors declare that they have no known competing financial interests or personal relationships that could have appeared to influence the work reported in this paper.

Acknowledgment

This work of Xiao Liu and Bin Yang was supported by the National Natural Science Foundation of China (52425605).

References

[1] Statistical review of world energy 2024. Report. London: Energy Institute; 2024.
[2] Escobar JC, Lora ES, Venturini OJ, Yáñez EE, Castillo EF, Almazan O. Biofuels: environment, technology and food security. Renew Sustain Energy Rev 2009;13(6–7):1275–87.
[3] State of the global climate 2023. Report. Geneva: World Meteorological Organization; 2023.
[4] Timilsina GR, Dulal H. A review of regulatory instruments to control environmental externalities from the transport sector. Report. Washington, DC: World Bank; 2009.
[5] Le Quéré C, Korsbakken JI, Wilson C, Tosun J, Andrew R, Andres RJ, et al. Drivers of declining CO_2 emissions in 18 developed economies. Nat Clim Change 2019;9(3):213–7.
[6] Usman A, Mohammed I, Dawaki KA. State of the art on vehicular engine exhaust emissions standards and regulations: a review. Traekt Nauki 2023;9(6):6001–9.
[7] Poudenx P. The effect of transportation policies on energy consumption and greenhouse gas emission from urban passenger transportation. Transp Res 2008;42(6):901–9.
[8] Twigg MV. Controlling automotive exhaust emissions: successes and underlying science. Philos Trans R Soc A 1829;2005(363):1013–33.
[9] Tripathi G, Dhar A, Sadiki A. Recent advancements in after-treatment technology for internal combustion engines—an overview. In: Srivastava D, Agarwal A, Datta A, Maurya R, editors. Advances in internal combustion engine research. Energy, environment, and sustainability. Singapore: Springer; 2018.
[10] Demirbaş A. Global renewable energy resources. Energy Sources A 2006;28(8):779–92.
[11] Notton G, Nivet ML, Voyant C, Paoli C, Darras C, Motte F, et al. Intermittent and stochastic character of renewable energy sources: consequences, cost of intermittence and benefit of forecasting. Renew Sustain Energy Rev 2018;87:96–105.
[12] Jin C, Li X, Xu T, Dong J, Geng Z, Liu J, et al. Zero-carbon and carbon-neutral fuels: a review of combustion products and cytotoxicity. Energies 2023;16:6507.
[13] Kalamaras E, Maroto-Valer MM, Shao M, Xuan J, Wang H. Solar carbon fuel via photoelectrochemistry. Catal Today 2018;317:56–75.
[14] Ababneh H, Hameed B. Electrofuels as emerging new green alternative fuel: a review of recent literature. Energy Convers Manage 2022;254:115213.
[15] Keasling J, Garcia Martin H, Lee TS, Mukhopadhyay A, Singer SW, Sundstrom E. Microbial production of advanced biofuels. Nat Rev Microbiol 2021;19(11):701–15.
[16] Khan N, Sudhakar K, Mamat R. Role of biofuels in energy transition, green economy and carbon neutrality. Sustainability 2021;13(22):12374.
[17] Rajagopal D. Implications of India's biofuel policies for food, water and the poor. Water Policy 2008;10(S1):95–106.
[18] Renewable energy market update 2021. Report. Paris: International Energy Agency; 2022.
[19] Gheewala SH, Damen B, Shi X. Biofuels: economic, environmental and social benefits and costs for developing countries in Asia. Wiley Interdiscip Rev Clim Change 2013;4(6):497–511.
[20] Balat M, Balat H. Progress in biodiesel processing. Appl Energy 2010;87(6):1815–35.
[21] Gasparatos A, Stromberg P, Takeuchi K. Sustainability impacts of first-generation biofuels. Anim Front 2013;3(2):12–26.
[22] Cherubini F, Strømman AH. Life cycle assessment of bioenergy systems: state of the art and future challenges. Bioresour Technol 2011;102(2):437–51.
[23] Popp J, Lakner Z, Harangi-Rákos M, Fári M. The effect of bioenergy expansion: food, energy, and environment. Renew Sustain Energy Rev 2014;32:559–78.
[24] Christopher LP, Kumar H, Zambare V. Enzymatic biodiesel: challenges and opportunities. Appl Energy 2014;119:497–520.
[25] Gupta VK, Potumarthi R, O'Donovan A, Kubicek CP, Sharma GD, Tuohy MG. Bioenergy research: an overview on technological developments and bioresources. Bioenergy research: advances and applications. Amsterdam: Elsevier; 2014.
[26] Sims RE, Mabee W, Saddler JN, Taylor M. An overview of second generation biofuel technologies. Bioresour Technol 2010;101(6):1570–80.
[27] Yue D, You F, Snyder SW. Biomass-to-bioenergy and biofuel supply chain optimization: overview, key issues and challenges. Comput Chem Eng 2014;66:36–56.
[28] Chen CY, Yeh KL, Aisyah R, Lee DJ, Chang JS. Cultivation, photobioreactor design and harvesting of microalgae for biodiesel production: a critical review. Bioresour Technol 2011;102(1):71–81.
[29] Pittman JK, Dean AP, Osundeko O. The potential of sustainable algal biofuel production using wastewater resources. Bioresour Technol 2011;102(1):17–25.
[30] Chisti Y. Biodiesel from microalgae. Biotechnol Adv 2007;25(3):294–306.

[31] Maeda Y, Yoshino T, Matsunaga T, Matsumoto M, Tanaka T. Marine microalgae for production of biofuels and chemicals. Curr Opin Biotechnol 2018;50:111–20.
[32] Park S, Nguyen THT, Jin E. Improving lipid production by strain development in microalgae: strategies, challenges and perspectives. Bioresour Technol 2019;292:121953.
[33] Wang Q, Lu Y, Xin Y, Wei L, Huang S, Xu J. Genome editing of model oleaginous microalgae nannochloropsis spp. by Crispr/Cas9. Plant J 2016;88 (6):1071–81.
[34] Greiner A, Kelterborn S, Evers H, Kreimer G, Sizova I, Hegemann P. Targeting of photoreceptor genes in chlamydomonas reinhardtii via zinc-finger nucleases and Crispr/Cas9. Plant Cell 2017;29(10):2498.
[35] Tran LS, Sirjean B, Glaude PA, Fournet R, Battin-Leclerc F. Progress in detailed kinetic modeling of the combustion of oxygenated components of biofuels. Energy 2012;43(1):4–18.
[36] Rorrer JE, Bell AT, Toste FD. Synthesis of biomass-derived ethers for use as fuels and lubricants. ChemSusChem 2019;12(13):2835–58.
[37] Li H, Riisager A, Saravanamurugan S, Pandey A, Sangwan RS, Yang S, et al. Carbon-increasing catalytic strategies for upgrading biomass into energy-intensive fuels and chemicals. ACS Catal 2018;8(1):148–87.
[38] Sreekumar S, Baer ZC, Pazhamalai A, Gunbas G, Grippo A, Blanch HW, et al. Production of an acetone–butanol–ethanol mixture from clostridium acetobutylicum and its conversion to high-value biofuels. Nat Protoc 2015;10(3):528–37.
[39] Serrano-Ruiz JC, West RM, Dumesic JA. Catalytic conversion of renewable biomass resources to fuels and chemicals. Annu Rev Chem Biomol Eng 2010;1 (1):79–100.
[40] O'Neill MF, Sankar M, Hintermair U. Sustainable synthesis of dimethyl and diethyl carbonate from CO_2 in batch and continuous flow—lessons from thermodynamics and the importance of catalyst stability. ACS Sustain Chem Eng 2022;10(16):5243–57.
[41] Kim D, Lee M, Shin Y, Lee J, Lee JW. Direct production of diethyl carbonate from ethylene carbonate and ethanol by energy-efficient intensification of reaction and separation. Chem Eng Process 2023;192:109519.
[42] Rong D, Zhang G, Sun Q, Hu X. Experimental study on gas production characteristics of electrolyte of lithium-ion battery under pyrolysis conditions. J Energy Storage 2023;74:109367.
[43] Hou J, Lu L, Wang L, Ohma A, Ren D, Feng X, et al. Thermal runaway of lithium-ion batteries employing Lin $(SO_2f)_2$-based concentrated electrolytes. Nat Commun 2020;11(1):5100.
[44] Xie H, Sun J, Li J, Zhou T, Wei S, Yi Z. Lithium-ion battery thermal runaway electro–thermal triggering method and toxicity analysis. Earth Environ Sci 2021;701:012007.
[45] Kohse-Höinghaus K. Combustion, chemistry, and carbon neutrality. Chem Rev 2023;123(8):5139–219.
[46] Dunphy MP, Patterson PM, Simmie JM. High-temperature oxidation of ethanol. Part 2. Kinetic modelling. J Chem Soc 1991;87(16):2549–59.
[47] Norton T, Dryer F. An experimental and modeling study of ethanol oxidation kinetics in an atmospheric pressure flow reactor. Int J Chem Kinet 1992;24 (4):319–44.
[48] Marinov NM. A detailed chemical kinetic model for high temperature ethanol oxidation. Int J Chem Kinet 1999;31(3):183–220.
[49] Göransson K, Söderlind U, He J, Zhang W. Review of syngas production via biomass DFBGs. Renew Sustain Energy Rev 2011;15(1):482–92.
[50] Nielsen HB, Heiske S. Anaerobic digestion of macroalgae: methane potentials, pre-treatment, inhibition and co-digestion. Water Sci Technol 2011;64 (8):1723–9.
[51] Battin-Leclerc F, Simmie JM, Blurock E. Cleaner combustion developing detailed chemical kinetic models preface. Green energy and technology. Cham: Springer International Publishing; 2013.
[52] Arrhenius S. Über die reaktionsgeschwindigkeit bei der inversion von rohrzucker durch säuren. Z Phys Chem 1889;4U(1):226–48.
[53] Gilbert R, Luther K, Troe J. Theory of thermal unimolecular reactions in the fall-off range. II. Weak collision rate constants. Berichte der Bunsengesellschaft für physikalische Chemie 1983;87(2):169–77.
[54] Zeleznik FJ. A general IBM 704 or 7090 computer program for computation of chemical equilibrium compositions, rocket performance, and chapman-jouguet dentonations. Report. Washington, DC: National Aeronautics and Space Administration; 1962.
[55] Kee RJ, Rupley FM, Miller JA. Chemkin-ii: a Fortran chemical kinetics package for the analysis of gas-phase chemical kinetics. Report. 1989.
[56] Goodwin DG, Moffat HK, Speth RL. Cantera: an object-oriented software toolkit for chemical kinetics, thermodynamics, and transport processes. Report. Zenodo; 2017.
[57] Cuoci A, Frassoldati A, Faravelli T, Opensmoke RE. Numerical modeling of reacting systems with detailed kinetic mechanisms. In: Proceedings of XXXIV Meeting of the Italian Section of the Combustion Institute, 2011.
[58] Curran HJ. Developing detailed chemical kinetic mechanisms for fuel combustion. Proc Combust Inst 2019;37(1):57–81.
[59] Smith GP, Golden DM, Frenklach M, Moriarty NW, Eiteneer B, Goldenberg M, et al. Gri-mech version 3.0. Software; 1999.
[60] Wang H, You X, Joshi AV, Davis SG, Laskin A, Egolfopoulos F, et al. High-temperature combustion reaction model of H2/CO/C1–C4 compounds [Internet]. [cited 2025 Mar 12]. Available from: http://ignis.usc.edu/USC_Mech_II.htm.
[61] Zhang Y, Vandewalle WDL, Xu R, Smith GP, Wang H. Foundational fuel chemistry model version 2.0 (FFCM-2) [Internet]. Stanford: FFCM-2 website; 2023 [cited 2025 Apr 2]. Available from: https://web.stanford.edu/group/haiwanglab/FFCM2.
[62] Wu Y, Panigrahy S, Sahu AB, Bariki C, Beeckmann J, Liang J, et al. Understanding the antagonistic effect of methanol as a component in surrogate fuel models: a case study of methanol/n-heptane mixtures. Combust Flame 2021;226:229–42.
[63] Zhou CW, Li Y, O'Connor E, Somers KP, Thion S, Keesee C, et al. A comprehensive experimental and modeling study of isobutene oxidation. Combust Flame 2016;167:353–79.
[64] Metcalfe WK, Burke SM, Ahmed SS, Curran HJ. A hierarchical and comparative kinetic modeling study of C1–C2 hydrocarbon and oxygenated fuels. Int J Chem Kinet 2013;45(10):638–75.
[65] Li Y, Zhou CW, Somers KP, Zhang K, Curran HJ. The oxidation of 2-butene: a high pressure ignition delay, kinetic modeling study and reactivity comparison with isobutene and 1-butene. Proc Combust Inst 2017;36 (1):403–11.
[66] Zádor J, Taatjes CA, Fernandes RX. Kinetics of elementary reactions in low-temperature autoignition chemistry. Pror Energy Combust Sci 2011;37 (4):371–421.
[67] Curran HJ, Gaffuri P, Pitz WJ, Westbrook CK. A comprehensive modeling study of iso-octane oxidation. Combust Flame 2002;129(3):253–80.
[68] Sarathy SM, Westbrook CK, Mehl M, Pitz WJ, Togbe C, Dagaut P, et al. Comprehensive chemical kinetic modeling of the oxidation of 2-methylalkanes from C7 to C20. Combust Flame 2011;158(12):2338–57.
[69] Westbrook CK, Pitz WJ, Herbinet O, Curran HJ, Silke EJ. A comprehensive detailed chemical kinetic reaction mechanism for combustion of *n*-alkane hydrocarbons from *n*-octane to *n*-hexadecane. Combust Flame 2009;156 (1):181–99.
[70] Battin-Leclerc F. Detailed chemical kinetic models for the low-temperature combustion of hydrocarbons with application to gasoline and diesel fuel surrogates. Pror Energy Combust Sci 2008;34(4):440–98.
[71] Villano SM, Huynh LK, Carstensen HH, Dean AM. High-pressure rate rules for alkyl+ O_2 reactions. 1. The dissociation, concerted elimination, and isomerization channels of the alkyl peroxy radical. J Phys Chem A 2011;115 (46):13425–42.
[72] Villano SM, Huynh LK, Carstensen HH, Dean AM. High-pressure rate rules for alkyl+ O_2 reactions. 2. The isomerization, cyclic ether formation, and β-scission reactions of hydroperoxy alkyl radicals. J Phys Chem A 2012;116 (21):5068–89.
[73] Sharma S, Raman S, Green WH. Intramolecular hydrogen migration in alkylperoxy and hydroperoxyalkylperoxy radicals: accurate treatment of hindered rotors. J Phys Chem A 2010;114(18):5689–701.
[74] Bugler J, Power J, Curran HJ. A theoretical study of cyclic ether formation reactions. Proc Combust Inst 2017;36(1):161–7.
[75] Bhaskaran K, Roth P. The shock tube as wave reactor for kinetic studies and material systems. Pror Energy Combust Sci 2002;28(2):151–92.
[76] Davidson DF, Hanson RK. Interpreting shock tube ignition data. Int J Chem Kinet 2004;36(9):510–23.
[77] Tranter R, Lynch P. A miniature high repetition rate shock tube. Rev Sci Instrum 2013;84(9):094102.
[78] Bugler J, Marks B, Mathieu O, Archuleta R, Camou A, Grégoire C, et al. An ignition delay time and chemical kinetic modeling study of the pentane isomers. Combust Flame 2016;163:138–56.
[79] Brett L, MacNamara J, Musch P, Simmie J. Simulation of methane autoignition in a rapid compression machine with creviced pistons. Combust Flame 2001;124(1–2):326–9.
[80] Zhang P, Li S, Wang Y, Ji W, Sun W, Yang B, et al. Measurement of reaction rate constants using RCM: a case study of decomposition of dimethyl carbonate to dimethyl ether. Combust Flame 2017;183:30–8.
[81] Battin-Leclerc F, Herbinet O, Glaude PA, Fournet R, Zhou Z, Deng L, et al. Experimental confirmation of the low-temperature oxidation scheme of alkanes. Angew Chem 2010;122(18):3237–40.
[82] Dryer FL, Haas FM, Santner J, Farouk TI, Chaos M. Interpreting chemical kinetics from complex reaction–advection–diffusion systems: modeling of flow reactors and related experiments. Pror Energy Combust Sci 2014;44:19–39.
[83] Park SH, Lee KM, Hwang CH. Effects of hydrogen addition on soot formation and oxidation in laminar premixed C_2H_2/air flames. Int J Hydrogen Energy 2011;36(15):9304–11.
[84] Wagner S, Klein M, Kathrotia T, Riedel U, Kissel T, Dreizler A, et al. Absolute, spatially resolved, *in situ* co profiles in atmospheric laminar counter-flow diffusion flames using 2.3 μm TDLAS. Appl Phys B 2012;109 (3):533–40.
[85] Goldsborough SS, Hochgreb S, Vanhove G, Wooldridge MS, Curran HJ, Sung CJ. Advances in rapid compression machine studies of low- and intermediate-temperature autoignition phenomena. Pror Energy Combust Sci 2017;63:631–78.
[86] Zhao H, Yan C, Zhang T, Ma G, Souza MJ, Zhou C, et al. Studies of high-pressure n-butane oxidation with CO_2 dilution up to 100 atm using a supercritical-pressure jet-stirred reactor. Proc Combust Inst 2021;38(1):279–87.
[87] Kang S, Liao W, Chu Z, Yang B. A rapid compression machine coupled with time-resolved molecular beam mass spectrometry for gas-phase kinetics studies. Rev Sci Instrum 2021;92(8):084103.

[88] Wolfrum J. Lasers in combustion: from basic theory to practical devices. Symp Combust 1998;27(1):1–41.
[89] Kohse-Höinghaus K, Barlow RS, Aldén M, Wolfrum J. Combustion at the focus: laser diagnostics and control. Proc Combust Inst 2005;30(1):89–123.
[90] Goldenstein CS, Spearrin RM, Jeffries JB, Hanson RK. Infrared laser-absorption sensing for combustion gases. Pror Energy Combust Sci 2017;60:132–76.
[91] Hansen N, Cool TA, Westmoreland PR, Kohse-Höinghaus K. Recent contributions of flame-sampling molecular-beam mass spectrometry to a fundamental understanding of combustion chemistry. Pror Energy Combust Sci 2009;35(2):168–91.
[92] Qi F. Combustion chemistry probed by synchrotron VUV photoionization mass spectrometry. Proc Combust Inst 2013;34(1):33–63.
[93] Liao W, Chu Z, Wang Y, Yang B. A kinetic investigation on low-temperature ignition of propane with ozone addition in an RCM. Proc Combust Inst 2023;39(1):395–403.
[94] Taatjes CA, Hansen N, Osborn DL, Kohse-Höinghaus K, Cool TA, Westmoreland PR. "Imaging" combustion chemistry via multiplexed synchrotron-photoionization mass spectrometry. Phys Chem Chem Phys 2008;10(1):20–34.
[95] Moshammer K, Jasper AW, Popolan-Vaida DM, Lucassen A, Diévart P, Selim H, et al. Detection and identification of the keto-hydroperoxide ($HOOCH_2OCHO$) and other intermediates during low-temperature oxidation of dimethyl ether. J Phys Chem A 2015;119(28):7361–74.
[96] Moshammer K, Jasper AW, Popolan-Vaida DM, Wang Z, Bhavani Shankar VS, Ruwe L, et al. Quantification of the keto-hydroperoxide ($HOOCH_2OCHO$) and other elusive intermediates during low-temperature oxidation of dimethyl ether. J Phys Chem A 2016;120(40):7890–901.
[97] Frenklach M. Transforming data into knowledge—process informatics for combustion chemistry. Proc Combust Inst 2007;31(1):125–40.
[98] Varga T, Olm C, Nagy T, Zsély IG, Valkó É, Pálvölgyi R, et al. Development of a joint hydrogen and syngas combustion mechanism based on an optimization approach. Int J Chem Kinet 2016;48(8):407–22.
[99] Olm C, Varga T, Valkó É, Curran HJ, Turányi T. Uncertainty quantification of a newly optimized methanol and formaldehyde combustion mechanism. Combust Flame 2017;186:45–64.
[100] Liu C, Lin K, Wang Y, Yang B. Multi-fidelity neural network for uncertainty quantification of chemical reaction models. Combust Flame 2023;258:113074.
[101] Lin K, Zhou Z, Law CK, Yang B. Dimensionality reduction for surrogate model construction for global sensitivity analysis: comparison between active subspace and local sensitivity analysis. Combust Flame 2021;232:111501.
[102] Sheen DA. Mumpce_py: a python implementation of the method of uncertainty minimization using polynomial chaos expansions. J Res Natl Inst Stand Technol 2017;122:39.
[103] Sheen DA, Wang H. The method of uncertainty quantification and minimization using polynomial chaos expansions. Combust Flame 2011;158(12):2358–74.
[104] Nagy T, Valkó É, Sedyó I, Zsély IG, Pilling MJ, Turányi T. Uncertainty of the rate parameters of several important elementary reactions of the H_2 and syngas combustion systems. Combust Flame 2015;162(5):2059–76.
[105] Nagy T, Turányi T. Uncertainty of arrhenius parameters. Int J Chem Kinet 2011;43(7):359–78.
[106] Kovács M, Papp M, Zsély IG, Turányi T. Main sources of uncertainty in recent methanol/NO_x combustion models. Int J Chem Kinet 2021;53(7):884–900.
[107] Olm C, Zsély IG, Pálvölgyi R, Varga T, Nagy T, Curran HJ, et al. Comparison of the performance of several recent hydrogen combustion mechanisms. Combust Flame 2014;161(9):2219–34.
[108] Tomlin AS. The role of sensitivity and uncertainty analysis in combustion modelling. Proc Combust Inst 2013;34(1):159–76.
[109] Ziehn T, Tomlin AS. GUI–HDMR—a software tool for global sensitivity analysis of complex models. Environ Model Softw 2009;24(7):775–85.
[110] Huan X, Marzouk YM. Simulation-based optimal Bayesian experimental design for nonlinear systems. J Comput Phys 2013;232(1):288–317.
[111] Sheen DA, Manion JA. Kinetics of the reactions of H and CH_3 radicals with *n*-butane: an experimental design study using reaction network analysis. J Phys Chem A 2014;118(27):4929–41.
[112] Valkó É, Papp M, Kovács M, Varga T, Zsély IG, Nagy T, et al. Design of combustion experiments using differential entropy. Combust Theory Modell 2022;26(1):67–90.
[113] Vom Lehn F, Cai L, Pitsch H. Iterative model-based experimental design for efficient uncertainty minimization of chemical mechanisms. Proc Combust Inst 2021;38(1):1033–42.
[114] Zhou Z, Lin K, Wang Y, Wang J, Law CK, Yang B. OptEx: an integrated framework for experimental design and combustion kinetic model optimization. Combust Flame 2022;245:112298.
[115] Cooke D, Dodson M, Williams A. A shock-tube study of the ignition of methanol and ethanol with oxygen. Combust Flame 1971;16(3):233–6.
[116] Smith SR, Gordon AS. Studies of diffusion flames. II. Diffusion flames of some simple alcohols. J Phys Chem 1956;60(8):1059–62.
[117] Bowman CT. A shock-tube investigation of the high-temperature oxidation of methanol. Combust Flame 1975;25:343–54.
[118] Norton T, Dryer F. Toward a comprehensive mechanism for methanol pyrolysis. Int J Chem Kinet 1990;22(3):219–41.
[119] Li J, Kazakov A, Dryer FL. Experimental and numerical studies of ethanol decomposition reactions. J Phys Chem A 2004;108(38):7671–80.
[120] Sarathy SM, Oβwald P, Hansen N, Kohse-Höinghaus K. Alcohol combustion chemistry. Pror Energy Combust Sci 2014;44:40–102.
[121] Zhang X, Wang G, Zou J, Li Y, Li W, Li T, et al. Investigation on the oxidation chemistry of methanol in laminar premixed flames. Combust Flame 2017;180:20–31.
[122] Li J, Zhao Z, Kazakov A, Chaos M, Dryer FL, Scire Jr JJ. A comprehensive kinetic mechanism for CO, CH_2O, and CH_3OH combustion. Int J Chem Kinet 2007;39(3):109–36.
[123] Chemical-kinetic mechanisms for combustion applications [Internet]. [cited 2025 March 12]. Available from: http://combustion.ucsd.edu.
[124] Christensen M, Nilsson E, Konnov A. A systematically updated detailed kinetic model for CH_2O and CH_3OH combustion. Energy Fuels 2016;30(8):6709–26.
[125] Zhang Y, El-Merhubi H, Lefort B, Le Moyne L, Curran HJ, Kéromnès A. Probing the low-temperature chemistry of ethanol via the addition of dimethyl ether. Combust Flame 2018;190:74–86.
[126] Liao W, Kang S, Chu Z, Liu Z, Wang Y, Yang B. Exploring the low-temperature oxidation chemistry with ozone addition in an RCM: a case study on ethanol. Combust Flame 2022;237:111727.
[127] Zhang X, Hong C, Feng Z, Zhang Y, Huang Z, Zhang Y. An ultraviolet laser absorption diagnostic for ȮH concentration time-history in ethanol oxidation and model improvement. Combust Flame 2024;261:113287.
[128] Pinzón LT, Mathieu O, Mulvihill CR, Schoegl I, Petersen EL. Ethanol pyrolysis kinetics using H_2O time history measurements behind reflected shock waves. Proc Combust Inst 2019;37(1):239–47.
[129] Kiecherer J, Bänsch C, Bentz T, Olzmann M. Pyrolysis of ethanol: a shock-tube/TOF-MS and modeling study. Proc Combust Inst 2015;35(1):465–72.
[130] Tao Y, Smith GP, Wang H. Critical kinetic uncertainties in modeling hydrogen/carbon monoxide, methane, methanol, formaldehyde, and ethylene combustion. Combust Flame 2018;195:18–29.
[131] Xing L, Li S, Wang Z, Yang B, Klippenstein SJ, Zhang F. Global uncertainty analysis for RRKM/master equation based kinetic predictions: a case study of ethanol decomposition. Combust Flame 2015;162(9):3427–36.
[132] Man X, Tang C, Zhang J, Zhang Y, Pan L, Huang Z, et al. An experimental and kinetic modeling study of *n*-propanol and *i*-propanol ignition at high temperatures. Combust Flame 2014;161(3):644–56.
[133] Zhang Z, Li A, Ma Z, Zhu L, Huang Z. An experimental and kinetic modeling study on the effects of molecular structure on oxidation of propanol isomers at engine-relevant condition in a variable pressure laminar flow reactor. Chem Eng Sci 2023;265:118241.
[134] Cooper SP, Grégoire CM, Mohr DJ, Mathieu O, Alturaifi SA, Petersen EL. An experimental kinetics study of isopropanol pyrolysis and oxidation behind reflected shock waves. Energies 2021;14(20):6808.
[135] Li W, Zhang Y, Mei B, Li Y, Cao C, Zou J, et al. Experimental and kinetic modeling study of *n*-propanol and *i*-propanol combustion: flow reactor pyrolysis and laminar flame propagation. Combust Flame 2019;207:171–85.
[136] Feng Y, Zhu J, Wang S, Yu L, He Z, Qian Y, et al. Theoretical and experimental study of 3-pentanol autoignition: *ab initio* calculation, shock tube experiments, and kinetic modeling. J Phys Chem A 2021;125(27):5976–89.
[137] Zhang K, Sawaya MR, Eisenberg DS, Liao JC. Expanding metabolism for biosynthesis of nonnatural alcohols. Proc Natl Acad Sci USA 2008;105(52):20653–8.
[138] Cann AF, Liao JC. Pentanol isomer synthesis in engineered microorganisms. Appl Microbiol Biotechnol 2010;858:93–9.
[139] Sarathy SM, Vranckx S, Yasunaga K, Mehl M, Oßwald P, Metcalfe WK, et al. A comprehensive chemical kinetic combustion model for the four butanol isomers. Combust Flame 2012;159(6):2028–55.
[140] Togbé C, Halter F, Foucher F, Mounaim-Rousselle C, Dagaut P. Experimental and detailed kinetic modeling study of 1-pentanol oxidation in a JSR and combustion in a bomb. Proc Combust Inst 2011;33(1):367–74.
[141] Heufer KA, Sarathy SM, Curran HJ, Davis AC, Westbrook CK, Pitz WJ. Detailed kinetic modeling study of *n*-pentanol oxidation. Energy Fuels 2012;26(11):6678–85.
[142] Köhler M, Kathrotia T, Oßwald P, Fischer-Tammer ML, Moshammer K, Riedel U. 1-, 2- and 3-pentanol combustion in laminar hydrogen flames—a comparative experimental and modeling study. Combust Flame 2015;162(9):3197–209.
[143] Chatterjee T, Saggese C, Dong S, Patel V, Lockwood KS, Curran HJ, et al. Experimental and kinetic modeling study of the low-temperature and high-pressure combustion chemistry of straight chain pentanol isomers: 1-, 2- and 3-pentanol. Proc Combust Inst 2023;39(1):265–74.
[144] Carbonnier M, Serinyel Z, Keromnes A, Dayma G, Lefort B, Le Moyne L, et al. An experimental and modeling study of the oxidation of 3-pentanol at high pressure. Proc Combust Inst 2019;37(1):477–84.
[145] Liu B, Zhu Q, Zhu L, Xie C, Xu Q, Wang Z. Low-temperature oxidation of n-butanol in a jet-stirred reactor: detailed species measurements and modeling studies. Combust Flame 2024;261:113290.
[146] Hashemi H, Christensen JM, Glarborg P. High-pressure pyrolysis and oxidation of ethanol. Fuel 2018;218:247–57.
[147] Weber BW, Merchant S, Sung CJ, Green WH. An autoignition study of iso-butanol: experiments and modeling. 2017. arXiv:1706.01827.
[148] Nativel D, Pelucchi M, Frassoldati A, Comandini A, Cuoci A, Ranzi E, et al. Laminar flame speeds of pentanol isomers: an experimental and modeling study. Combust Flame 2016;166:1–18.
[149] Cai L, Kröger L, Döntgen M, Leonhard K, Narayanaswamy K, Sarathy SM, et al. Exploring the combustion chemistry of a novel lignocellulose-derived

biofuel: cyclopentanol. Part i: quantum chemistry calculation and kinetic modeling. Combust Flame 2019;210:490–501.
[150] Pelucchi M, Namysl S, Ranzi E, Rodriguez A, Rizzo C, Somers K, et al. Combustion of n-C3–C6 linear alcohols: an experimental and kinetic modeling study. Part ii: speciation measurements in a jet-stirred reactor, ignition delay time measurements in a rapid compression machine, model validation, and kinetic analysis. Energy Fuels 2020;34(11):14708–25.
[151] Herrmann F, Jochim B, Oßwald P, Cai L, Pitsch H, Kohse-Höinghaus K. Experimental and numerical low-temperature oxidation study of ethanol and dimethyl ether. Combust Flame 2014;161(2):384–97.
[152] Demirbas A. Progress and recent trends in biodiesel fuels. Energy Convers Manage 2009;50(1):14–34.
[153] Lai JY, Lin KC, Violi A. Biodiesel combustion: advances in chemical kinetic modeling. Pror Energy Combust Sci 2011;37(1):1–14.
[154] Herbinet O, Pitz WJ, Westbrook CK. Detailed chemical kinetic mechanism for the oxidation of biodiesel fuels blend surrogate. Combust Flame 2010;157(5):893–908.
[155] Westbrook C, Pitz W, Sarathy S, Mehl M. Detailed chemical kinetic modeling of the effects of CC double bonds on the ignition of biodiesel fuels. Proc Combust Inst 2013;34(2):3049–56.
[156] Zhou W, Wang Z, Liang Y, Zhang X, Yu L, Lu X. The effect of the unsaturation degree on the gas-phase autoignition of methyl oleate and methyl linoleate: experimental and modeling study. Combust Flame 2024;263:113381.
[157] Glaude PA, Pitz WJ, Thomson MJ. Chemical kinetic modeling of dimethyl carbonate in an opposed-flow diffusion flame. Proc Combust Inst 2005;30(1):111–8.
[158] Zhao L, Xie M, Ye L, Cheng Z, Cai J, Li Y, et al. An experimental and modeling study of methyl propanoate pyrolysis at low pressure. Combust Flame 2013;160(10):1958–66.
[159] Herbinet O, Biet J, Hakka MH, Warth V, Glaude PA, Nicolle A, et al. Modeling study of the low-temperature oxidation of large methyl esters from C11 to C19. Proc Combust Inst 2011;33(1):391–8.
[160] Fisher EM, Pitz WJ, Curran HJ, Westbrook CK. Detailed chemical kinetic mechanisms for combustion of oxygenated fuels. Proc Combust Inst 2000;28(2):1579–86.
[161] Dooley S, Curran HJ, Simmie JM. Autoignition measurements and a validated kinetic model for the biodiesel surrogate, methyl butanoate. Combust Flame 2008;153(1–2):2–32.
[162] Gaïl S, Sarathy SM, Thomson MJ, Diévart P, Dagaut P. Experimental and chemical kinetic modeling study of small methyl esters oxidation: methyl (E)-2-butenoate and methyl butanoate. Combust Flame 2008;155(4):635–50.
[163] Hakka MH, Bennadji H, Biet J, Yahyaoui M, Sirjean B, Warth V, et al. Oxidation of methyl and ethyl butanoates. Int J Chem Kinet 2010;42(4):226–52.
[164] Lele AD, Vallabhuni SK, Moshammer K, Fernandes RX, Krishnasamy A, Narayanaswamy K. Experimental and chemical kinetic modeling investigation of methyl butanoate as a component of biodiesel surrogate. Combust Flame 2018;197:49–64.
[165] Herbinet O, Pitz WJ, Westbrook CK. Detailed chemical kinetic oxidation mechanism for a biodiesel surrogate. Combust Flame 2008;154(3):507–28.
[166] Glaude PA, Herbinet O, Bax S, Biet J, Warth V, Battin-Leclerc F. Modeling of the oxidation of methyl esters—validation for methyl hexanoate, methyl heptanoate, and methyl decanoate in a jet-stirred reactor. Combust Flame 2010;157(11):2035–50.
[167] Naik CV, Westbrook CK, Herbinet O, Pitz WJ, Mehl M. Detailed chemical kinetic reaction mechanism for biodiesel components methyl stearate and methyl oleate. Proc Combust Inst 2011;33(1):383–9.
[168] Zhou W, Liang Y, Pei X, Zhang Y, Yu L, Lu X. Autoignition of methyl palmitate in low to intermediate temperature: experiments in rapid compression machine and kinetic modeling. Combust Flame 2023;249:112619.
[169] Zhou W, Liang Y, Zhang Y, Wang Z, Yu L, Lu X. Experimental and modeling study on the autoignition characteristics of methyl stearate in a rapid compression machine. Combust Flame 2023;255:112942.
[170] Rodriguez A, Herbinet O, Battin-Leclerc F, Frassoldati A, Faravelli T, Ranzi E. Experimental and modeling investigation of the effect of the unsaturation degree on the gas-phase oxidation of fatty acid methyl esters found in biodiesel fuels. Combust Flame 2016;164:346–62.
[171] Li H, Yang W, Zhou D, Yu W. Skeletal mechanism construction for heavy saturated methyl esters in real biodiesel fuels. Fuel 2019;239:263–71.
[172] Zhang L, Qi Q, Wang Z, Ren G, Liu Z. Development of a reduced oxidation mechanism with low-temperature chemistry for real biodiesel methyl esters. Fuel 2023;338:127289.
[173] Wu G, Wang X, Abubakar S, Li Y, Liu Z. A realistic skeletal mechanism for the oxidation of biodiesel surrogate composed of long carbon chain and polyunsaturated compounds. Fuel 2021;289:119934.
[174] Westbrook CK, Naik CV, Herbinet O, Pitz WJ, Mehl M, Sarathy SM, et al. Detailed chemical kinetic reaction mechanisms for soy and rapeseed biodiesel fuels. Combust Flame 2011;158(4):742–55.
[175] Zhang X, Li W, Xu Q, Zhang Y, Jing Y, Wang Z, et al. A decoupled modeling approach and experimental measurements for pyrolysis of C6-C10 saturated fatty acid methyl esters (FAMEs). Combust Flame 2022;243:111955.
[176] Zhang X, Sarathy SM. High-temperature pyrolysis and combustion of C5–C19 fatty acid methyl esters (FAMEs): a lumped kinetic modeling study. Energy Fuels 2021;35(23):19553–67.
[177] McCormick RL, Fioroni G, Fouts L, Christensen E, Yanowitz J, Polikarpov E, et al. Selection criteria and screening of potential biomass-derived streams as fuel blend stocks for advanced spark-ignition engines. SAE Int J Fuel Lubr 2017;10(2):442–60.
[178] Hoppe F, Burke U, Thewes M, Heufer A, Kremer F, Pischinger S. Tailor-made fuels from biomass: potentials of 2-butanone and 2-methylfuran in direct injection spark ignition engines. Fuel 2016;167:106–17.
[179] Barak S, Rahman RK, Neupane S, Ninnemann E, Arafin F, Laich A, et al. Measuring the effectiveness of high-performance co-optima biofuels on suppressing soot formation at high temperature. Proc Natl Acad Sci USA 2020;117(7):3451–60.
[180] Hong C, Zhang X, Zou J, Huang Z, Zhang Y, Farooq A. Laser-based speciation of acetone oxidation behind reflected shock waves and chemical kinetic modeling. Int J Hydrogen Energy 2025;141:46–58.
[181] Burke U, Beeckmann J, Kopp WA, Uygun Y, Olivier H, Leonhard K, et al. A comprehensive experimental and kinetic modeling study of butanone. Combust Flame 2016;168:296–309.
[182] Yu D, Tian ZY, Wang Z, Liu YX, Zhou L. Experimental and theoretical study on acetone pyrolysis in a jet-stirred reactor. Fuel 2018;234:1380–7.
[183] Hemken C, Burke U, Lam KY, Davidson DF, Hanson RK, Heufer KA, et al. Toward a better understanding of 2-butanone oxidation: detailed species measurements and kinetic modeling. Combust Flame 2017;184:195–207.
[184] Thion S, Diévart P, Van Cauwenberghe P, Dayma G, Serinyel Z, Dagaut P. An experimental study in a jet-stirred reactor and a comprehensive kinetic mechanism for the oxidation of methyl ethyl ketone. Proc Combust Inst 2017;36(1):459–67.
[185] Fenard Y, Pieper J, Hemken C, Minwegen H, Büttgen RD, Kohse-Höinghaus K, et al. Experimental and modeling study of the low to high temperature oxidation of the linear pentanone isomers: 2-pentanone and 3-pentanone. Combust Flame 2020;216:29–44.
[186] Kang S, Liao W, Sun W, Lin K, Liao H, Moshammer K, et al. Exploring low-temperature oxidation chemistry of 2- and 3-pentanone. Combust Flame 2023;257:112561.
[187] Sun W, Tao T, Liao H, Hansen N, Yang B. Probing fuel-specific reaction intermediates from laminar premixed flames fueled by two C5 ketones and model interpretations. Proc Combust Inst 2019;37(2):1699–707.
[188] Pieper J, Hemken C, Büttgen R, Graf I, Hansen N, Heufer KA, et al. A high-temperature study of 2-pentanone oxidation: experiment and kinetic modeling. Proc Combust Inst 2019;37(2):1683–90.
[189] Li W, Mei B, Li Y, Eckart S, Krause H, Ma S, et al. Insight into fuel isomeric effects on laminar flame propagation of pentanones. Proc Combust Inst 2021;38(2):2135–42.
[190] Kang S, Huang C, Wang Y, Zhang P, Sun W, Law CK, et al. Isomer-specific influences on ignition and intermediates of two C5 ketones in an RCM. Proc Combust Inst 2021;38(2):2295–303.
[191] Meziane I, Fenard Y, Delort N, Herbinet O, Bourgalais J, Ramalingam A, et al. Experimental and modeling study of acetone combustion. Combust Flame 2023;257:112416.
[192] Liao H, Tao T, Sun W, Hansen N, Yang B. Isomer-specific speciation behaviors probed from premixed flames fueled by acetone and propanal. Proc Combust Inst 2021;38(2):2441–8.
[193] Decottignies V, Gasnot L, Pauwels J. A comprehensive chemical mechanism for the oxidation of methylethylketone in flame conditions. Combust Flame 2002;130(3):225–40.
[194] Zhang J, Li W, Mei B, Li Y. Laminar flame propagation of acetone and 2-butanone at normal to high pressures: insight into fuel molecular structure effects of ketones. Proc Combust Inst 2023;39(2):1709–20.
[195] Serinyel Z, Chaumeix N, Black G, Simmie J, Curran H. Experimental and chemical kinetic modeling study of 3-pentanone oxidation. J Phys Chem A 2010;114(46):12176–86.
[196] Dames EE, Lam KY, Davidson DF, Hanson RK. An improved kinetic mechanism for 3-pentanone pyrolysis and oxidation developed using multispecies time histories in shock-tubes. Combust Flame 2014;161(5):1135–45.
[197] Thion S, Togbé C, Dayma G, Serinyel Z, Dagaut P. Experimental and detailed kinetic modeling study of cyclopentanone oxidation in a jet-stirred reactor at 1 and 10 atm. Energy Fuels 2017;31(3):2144–55.
[198] Cheng J, Zou C, Lin Q, Liu S, Wang Y, Liu Y. High-temperature oxidation of methyl isopropyl ketone: a shock tube experiment and a kinetic model. Combust Flame 2019;209:376–88.
[199] Li W, Ye L, Fang Q, Zou J, Yang J, Li Y. Exploration on thermal decomposition of cyclopentanone: a flow reactor pyrolysis and kinetic modeling study. Energy Fuels 2021;35(17):14023–34.
[200] Lin Q, Chen J, Hu X, Zou C, Konnov AA. Measurements of laminar burning velocities and kinetic modelling of two symmetrical ketones: di-ethyl ketone and di-isopropyl ketone. Combust Flame 2024;268:113614.
[201] Serinyel Z, Togbé C, Zaras A, Dayma G, Dagaut P. Kinetics of oxidation of cyclohexanone in a jet-stirred reactor: experimental and modeling. Proc Combust Inst 2015;35(1):507–14.
[202] He J, Gou Y, Lu P, Zhang C, Li P, Li X. Shock tube measurements and kinetic modeling study on autoignition characteristics of cyclohexanone. Combust Flame 2018;192:358–68.
[203] Allen JW, Scheer AM, Gao CW, Merchant SS, Vasu SS, Welz O, et al. A coordinated investigation of the combustion chemistry of diisopropyl ketone, a prototype for biofuels produced by endophytic fungi. Combust Flame 2014;161(3):711–24.
[204] Barari G, Pryor O, Koroglu B, Sarathy SM, Masunov AE, Vasu SS. High temperature shock tube experiments and kinetic modeling study of diisopropyl ketone ignition and pyrolysis. Combust Flame 2017;177:207–18.

[205] Lin Q, Zou C, Luo J, Xia W, Li W, Peng C. A shock tube experiment and an improved high-temperature diisopropyl ketone model by Bayesian optimization. Combust Flame 2022;245:112305.
[206] Pichon S, Black G, Chaumeix N, Yahyaoui M, Simmie J, Curran H, et al. The combustion chemistry of a fuel tracer: measured flame speeds and ignition delays and a detailed chemical kinetic model for the oxidation of acetone. Combust Flame 2009;156(2):494–504.
[207] Sato K, Hidaka Y. Shock-tube and modeling study of acetone pyrolysis and oxidation. Combust Flame 2000;122(3):291–311.
[208] Serinyel Z, Black G, Curran H, Simmie J. A shock tube and chemical kinetic modeling study of methy ethyl ketone oxidation. Combust Sci Technol 2010;182(4–6):574–87.
[209] Kuzhanthaivelan S, Rajakumar B. Computational investigations on the thermochemistry and kinetics for the autoignition of 2-pentanone. Combust Flame 2020;219:147–60.
[210] Scheer AM, Eskola AJ, Osborn DL, Sheps L, Taatjes CA. Resonance stabilization effects on ketone autoxidation: isomer-specific cyclic ether and ketohydroperoxide formation in the low-temperature (400–625 K) oxidation of diethyl ketone. J Phys Chem A 2016;120(43):8625–36.
[211] Scheer AM, Welz O, Zádor J, Osborn DL, Taatjes CA. A Low-temperature combustion chemistry of novel biofuels: resonance-stabilized QOOH in the oxidation of diethyl ketone. Phys Chem Chem Phys 2014;16(26):13027–40.
[212] Minwegen H, Burke U, Heufer KA. An experimental and theoretical comparison of C3–C5 linear ketones. Proc Combust Inst 2017;36(1):561–8.
[213] Arteconi A, Mazzarini A, Di Nicola G. Emissions from ethers and organic carbonate fuel additives: a review. Water Air Soil Pollut 2011;221(1–4):405–23.
[214] Dagaut P, Boettner JC, Cathonnet M. Chemical kinetic study of dimethylether oxidation in a jet stirred reactor from 1 to 10 atm: experiments and kinetic modeling. Symp Combust 1996;26(1):627–32.
[215] Burke U, Somers KP, O'Toole P, Zinner CM, Marquet N, Bourque G, et al. An ignition delay and kinetic modeling study of methane, dimethyl ether, and their mixtures at high pressures. Combust Flame 2015;162(2):315–30.
[216] Wang Z, Zhang X, Xing L, Zhang L, Herrmann F, Moshammer K, et al. Experimental and kinetic modeling study of the low-and intermediate-temperature oxidation of dimethyl ether. Combust Flame 2015;162(4):1113–25.
[217] Stagni A, Schmitt S, Pelucchi M, Frassoldati A, Kohse-Höinghaus K, Faravelli T. Dimethyl ether oxidation analyzed in a given flow reactor: experimental and modeling uncertainties. Combust Flame 2022;240:111998.
[218] Tran LS, Herbinet O, Li Y, Wullenkord J, Zeng M, Bräuer E, et al. Low-temperature gas-phase oxidation of diethyl ether: fuel reactivity and fuel-specific products. Proc Combust Inst 2019;37(1):511–9.
[219] Fan X, Sun W, Gao Y, Hansen N, Chen B, Pitsch H, et al. Chemical insights into the multi-regime low-temperature oxidation of di-*n*-propyl ether: jet-stirred reactor experiments and kinetic modeling. Combust Flame 2021;233:111592.
[220] Thion S, Togbé C, Serinyel Z, Dayma G, Dagaut P. A chemical kinetic study of the oxidation of dibutyl-ether in a jet-stirred reactor. Combust Flame 2017;185:4–15.
[221] Fan X, Sun W, Liu Z, Gao Y, Yang J, Yang B, et al. Exploring the oxidation chemistry of diisopropyl ether: jet-stirred reactor experiments and kinetic modeling. Proc Combust Inst 2021;38(1):321–8.
[222] Serinyel Z, Lailliau M, Dayma G, Dagaut P. A high pressure oxidation study of di-*n*-propyl ether. Fuel 2020;263:116554.
[223] Zhang X, Feng Z, Hong C, Zhang Y, Huang Z, Zhang Y. Validation and improvement of dimethyl ether kinetic models: Insights from ȮH laser-absorption measurements across a wide pressure range. Combust Flame 2025;275:114048.
[224] Fan X, Hou Q, Sun W, Liu Z, Chen H, Yang J, et al. Oxidation of ethyl methyl ether: jet-stirred reactor experiments and kinetic modeling. Proc Combust Inst 2023;39(1):275–83.
[225] Serinyel Z, Lailliau M, Thion S, Dayma G, Dagaut P. An experimental chemical kinetic study of the oxidation of diethyl ether in a jet-stirred reactor and comprehensive modeling. Combust Flame 2018;193:453–62.
[226] Cheng Z, Wang H, Yin W, Wang J, Li W, Wang Z, et al. Experimental and kinetic modeling study of di-*n*-propyl ether and diisopropyl ether combustion: pyrolysis and laminar flame propagation velocity. Combust Flame 2022;237:111809.
[227] Cai L, Sudholt A, Lee DJ, Egolfopoulos FN, Pitsch H, Westbrook CK, et al. Chemical kinetic study of a novel lignocellulosic biofuel: di-*n*-butyl ether oxidation in a laminar flow reactor and flames. Combust Flame 2014;161(3):798–809.
[228] Hakimov K, Arafin F, Aljohani K, Djebbi K, Ninnemann E, Vasu SS, et al. Ignition delay time and speciation of dibutyl ether at high pressures. Combust Flame 2021;223:98–109.
[229] Jouzdani S, Zheng X, Zhou A, Akih-Kumgeh B. Shock tube investigation of methyl tert butyl ether and methyl tetrahydrofuran high-temperature kinetics. Int J Chem Kinet 2019;51(11):848–60.
[230] Hu E, Ku J, Yin G, Li C, Lu X, Huang Z. Laminar flame characteristics and kinetic modeling study of ethyl tertiary butyl ether compared with methyl tertiary butyl ether, ethanol, iso-octane, and gasoline. Energy Fuels 2018;32(3):3935–49.
[231] Tran LS, Verdicchio M, Monge F, Martin RC, Bounaceeur R, Sirjean B, et al. An experimental and modeling study of the combustion of tetrahydrofuran. Combust Flame 2015;162(5):1899–918.
[232] Xu N, Tang C, Meng X, Fan X, Tian Z, Huang Z. Experimental and kinetic study on the ignition delay times of 2, 5-dimethylfuran and the comparison to 2-methylfuran and furan. Energy Fuels 2015;29(8):5372–81.
[233] Cheng Z, Niu Q, Wang Z, Jin H, Chen G, Yao M, et al. Experimental and kinetic modeling studies of low-pressure premixed laminar 2-methylfuran flames. Proc Combust Inst 2017;36(1):1295–302.
[234] Fenard Y, Boumehdi MA, Vanhove G. Experimental and kinetic modeling study of 2-methyltetrahydrofuran oxidation under engine-relevant conditions. Combust Flame 2017;178:168–81.
[235] Fenard Y, Song H, Minwegen H, Parab P, Mergulhão CS, Vanhove G, et al. 2, 5-dimethyltetrahydrofuran combustion: Ignition delay times at high and low temperatures, speciation measurements and detailed kinetic modeling. Combust Flame 2019;203:341–51.
[236] Sun W, Wang G, Li S, Zhang R, Yang B, Yang J, et al. Speciation and the laminar burning velocities of poly (oxymethylene) dimethyl ether 3 (POMDME3) flames: an experimental and modeling study. Proc Combust Inst 2017;36(1):1269–78.
[237] He T, Wang Z, You X, Liu H, Wang Y, Li X, et al. A chemical kinetic mechanism for the low- and intermediate-temperature combustion of polyoxymethylene dimethyl ether 3 (PODE3). Fuel 2018;212:223–35.
[238] Román-Leshkov Y, Barrett CJ, Liu ZY, Dumesic JA. Production of dimethylfuran for liquid fuels from biomass-derived carbohydrates. Nature 2007;447:982–5.
[239] Yang W, Sen A. One-step catalytic transformation of carbohydrates and cellulosic biomass to 2, 5-dimethyltetrahydrofuran for liquid fuels. ChemSusChem 2010;3(5):597–603.
[240] Zheng Y, Tang Q, Wang T, Liao Y, Wang J. Synthesis of a green fuel additive over cation resins. Chem Eng Technol 2013;36(11):1951–6.
[241] Chen H, Wang H, Chen Z, Zhao H, Geng L, Gao N, et al. Research progress on the spray, combustion and emission of polyoxymethylene dimethyl ethers as a diesel blend fuel: a review. Fuel 2022;324:124731.
[242] Houache MS, Yim CH, Karkar Z, Abu-Lebdeh Y. On the current and future outlook of battery chemistries for electric vehicles—mini review. Batteries 2022;8(7):70.
[243] Rowden B, Garcia-Araez N. A review of gas evolution in lithium ion batteries. Energy Rep 2020;6:10–8.
[244] Wang Q, Jiang L, Yu Y, Sun J. Progress of enhancing the safety of lithium ion battery from the electrolyte aspect. Nano Energy 2019;55:93–114.
[245] Hu E, Chen Y, Zhang Z, Pan L, Li Q, Cheng Y, et al. Experimental and kinetic study on ignition delay times of dimethyl carbonate at high temperature. Fuel 2015;140:626–32.
[246] Sun W, Yang B, Hansen N, Westbrook CK, Zhang F, Wang G, et al. An experimental and kinetic modeling study on dimethyl carbonate (DMC) pyrolysis and combustion. Combust Flame 2016;164:224–38.
[247] Yu R, Liu J, Wu Y, Tang C, Liang W, Wang H, et al. Experimental and modeling study of the ignition kinetics of dimethyl carbonate. Combust Flame 2022;246:112465.
[248] Sun W, Huang C, Tao T, Zhang F, Li W, Hansen N, et al. Exploring the high-temperature kinetics of diethyl carbonate (DEC) under pyrolysis and flame conditions. Combust Flame 2017;181:71–81.
[249] Alexandrino K, Alzueta MU, Curran HJ. An experimental and modeling study of the ignition of dimethyl carbonate in shock tubes and rapid compression machine. Combust Flame 2018;188:212–26.
[250] Notario R, Quijano J, Sánchez C, Vélez E. Theoretical study of the mechanism of thermal decomposition of carbonate esters in the gas phase. J Phys Org Chem 2005;18(2):134–41.
[251] Nakamura H, Curran HJ, Córdoba AP, Pitz WJ, Dagaut P, Togbé C, et al. An experimental and modeling study of diethyl carbonate oxidation. Combust Flame 2015;162(4):1395–405.
[252] Zhao H, Liu S, Yan C, Huang C, Qi Y, Zhang F, et al. Studies of ozone-sensitized low-and high-temperature oxidations of diethyl carbonate. J Phys Chem A 2021;125(8):1760–5.
[253] Grégoire CM, Cooper SP, Khan-Ghauri M, Alturaifi SA, Petersen EL, Mathieu O. Pyrolysis study of dimethyl carbonate, diethyl carbonate, and ethyl methyl carbonate using shock-tube spectroscopic co measurements and chemical kinetics investigation. Combust Flame 2023;249:112594.
[254] Pokorny V, Stejfa V, Fulem M, Cervinka C, Ruzicka K. Vapor pressures and thermophysical properties of ethylene carbonate, propylene carbonate, γ-valerolactone, and γ-butyrolactone. J Chem Eng Data 2017;62(12):4174–86.
[255] Kanayama K, Grégoire CM, Cooper SP, Almarzooq Y, Petersen EL, Mathieu O, et al. Experimental and chemical kinetic modeling study of ethylene carbonate oxidation: a lithium-ion battery electrolyte surrogate model. Combust Flame 2024;262:113333.
[256] Dong B, Yu Y, Zhu Q, Liu B, Zhang K, Fang J, et al. Experimental study of ethylene carbonate (EC) pyrolysis and oxidation in jet-stirred reactor by SVUV-PIMS. Combust Flame 2025;274:114002.
[257] Kanayama K, Takahashi S, Nakamura H, Tezuka T, Maruta K. Experimental and modeling study on pyrolysis of ethylene carbonate/dimethyl carbonate mixture. Combust Flame 2022;245:112359.

[258] Cooper SP, Grégoire CM, Almarzooq YM, Petersen EL, Mathieu O. Experimental kinetics study on diethyl carbonate oxidation. Fuels 2023;4(2):243–60.
[259] Takahashi S, Kanayama K, Morikura S, Nakamura H, Tezuka T, Maruta K. Study on oxidation and pyrolysis of carbonate esters using a micro flow reactor with a controlled temperature profile. Part ii: chemical kinetic modeling of ethyl methyl carbonate. Combust Flame 2022;238:111878.
[260] Grégoire CM, Almarzooq YM, Petersen EL, Mathieu O. Experimental and modeling study of the combustion of ethyl methyl carbonate, a battery electrolyte. Combust Flame 2024;260:113225.
[261] Moc J, Simmie JM, Curran HJ. The elimination of water from a conformationally complex alcohol: a computational study of the gas phase dehydration of *n*-butanol. J Mol Struct 2009;928(1–3):149–57.